Title: Functional genetics of rice *PISTILLATA* genes unravels new roles and targets in flowering time, female fertility and parthenocarpy

Running Title: Roles of rice *PI* paralogs in floral development

Authors: Mohamed Zamzam[1,4], Ritabrata Basak[1#], Sharad Singh [1#], Sandhan Prakash [1#], Raghavaram Peesapati[1], Imtiyaz Khanday[1,3], Sara Simonini[2], Ueli Grossniklaus[2] and Usha Vijayraghavan*[1]

[1] Department of Microbiology and Cell Biology, Indian Institute of Science, Bangalore 560012, India

[2] Institute of Plant and Microbial Biology, University of Zurich, Zollikerstrasse 107, CH8008, Zurich, Switzerland

[3] Present address: Department of Plant Sciences, University of California, Davis, 95616, USA

[4]Present address: Branch of Genetics, Department of Agricultural Botany, Faculty of Agriculture at Cairo, Al-Azhar University, Cairo, 11651, Egypt, Visiting Faculty, Indian Institute of Science, Bangalore 560012, India

Shared second authors

*Corresponding author: Usha Vijayraghavan

Department of Microbiology and Cell Biology,

Indian Institute of Science, Bangalore 560012, India

Email: uvr@iisc.ac.in and uvr123@gmail.com

Tel.: +918023600168 14 Fax: +918023602697

Abstract

Diversification of transcription factors and of their downstream targets can contribute to new organ morphologies. An example is rice lodicule, a small fleshy petal homolog that aids floret opening, thus facilitates pollination and fertility. To understand mechanisms underlying its specification, we investigated the developmental functions of the rice *PISTILLATA* (*PI*) paralogs, *OsMADS2* and *OsMADS4.* Null *osmads2* mutants reiterated OsMADS2 nonredundant lodicule specification roles and revealed new roles in flowering time and floral organ number and fate. Doubly perturbed *osmads2*$^{d8/d8}$ *osmads4kd* florets had severe abnormalities, were female infertile, yet initiated parthenocarpy. Ubiquitous *OsMADS4* overexpression rescued *osmads2* abnormalities. Target genes whose regulation can contribute to OsMADS2 functions were discovered by its genome-wide binding analyses and transcriptome profiling. Several targets are implicated in lodicule and stamen development, floral organ number, cell wall, cell shape and osmotic homeostasis processes. Some targets relevant to lodicule development are cell division regulators (Cyclin D6, Cyclin P4-1-like), aquaporin (PIP1A), peptide transporter (PTR2), vascular development regulator (HOX1) and cell wall modulator (GH9B16). Their deregulation underscores the perturbed cell division, tissue differentiation patterns and physiology of the malformed *osmads2* and *osmads2*$^{d8/d8}$ *osmads4kd* lodicules. Altogether, we reveal novel roles for the rice *PI* paralogs in flowering time, panicle exsertion and embryo sac differentiation, divulge gene targets for lodicule development and provide mechanistic insights on the functional diversification of rice *PI* paralogs.

Keywords: *OsMADS2*; Rice *PISTILLATA*; lodicule and stamen development

Introduction

Floral organs in angiosperms are arranged in four concentric whorls. Their identity is controlled largely by the combinatorial action of homeotic transcription factors of the MIKC-type MADS-domain family (Lohmann and Weigel, 2002; Krizek and Fletcher, 2005). The ABC and the expanded ABCDE models of floral organ patterning, predict how five classes of homeotic transcription factors: A, B, C, D and E can pattern floral organs on the determinate floral meristem (Coen and Meyerowitz, 1991; Favaro et al., 2003; Pinyopich et al., 2003; Krizek and Fletcher, 2005). Although not strictly conserved across angiosperms, this model provides a baseline for gauging functional conservation *versus* divergence. The ABCDE model indicates that the specification of eudicot second and third whorl floral organs, petals and stamens, requires a pair of related B-class genes: *APETALA3* (*AP3*) and *PISTILLATA* (*PI*) in *Arabidopsis thaliana*, and *DEFICIENS* (*DEF*) and *GLOBOSA* (*GLO*) in *Antirrhinum majus* (Coen and Meyerowitz, 1991). Not surprisingly, studies in cereal models demonstrated that B-class genes are also required for specifying the identity of second and third whorl floral organs, lodicules and stamens (Ambrose et al., 2000; Nagasawa et al., 2003; Prasad and Vijayraghavan, 2003; Yadav et al., 2007). These reports support the interpretation that lodicules, in cereals and grasses, are eudicot petal homologs and indicate shared elements in the genetic control of lodicule and petal development. However, the remarkable morphological and functional differences of these organs indicate differences in their developmental pathways.

Rice genome constitutes two *PI* paralogs: *OsMADS2* and *OsMADS4* (Chung et al., 1995). The phenotypes of lodicules and stamens in single and double knockdown plants for these *PI*-clade genes, *i.e.*, *osmads2dsRNAi, osmads4dsRNAi*, and *osmads2- and osmads4-dsRNAi*, suggested their complete redundancy for stamen specification and unequal contribution for lodicule development (Prasad and Vijayraghavan, 2003; Yao et al., 2008). Yet, mechanisms underlying their unequal roles in lodicules are unknown.

The identification of DNA binding sites and target genes of transcription factors bring insights into their molecular functions. A previous study of our group, based on transcriptomic changes triggered by *OsMADS2* RNA interference-mediated gene silencing (RNAi), as detected by 22,000 probe-based microarrays, in a broad pool of developing floral tissues, showed that 9% of OsMADS2 targets had annotated functions in diverse aspects of cell division control and suggested a diversification compared to *Arabidopsis* PI (Yadav et al., 2007). Here, we first generated null alleles of *OsMADS2* by gene editing, carried out a detailed phenotypic analysis, and performed developmentally staged panicle transcriptome profiling. To unravel the gene

76 regulatory networks underlying the sub-functionalized activities of OsMADS2, this
77 transcriptome analysis was coupled with a determination of its genome-wide DNA occupancy
78 in developing florets. Furthermore, we generated *osmads2 osmads4kd* plants, doubly
79 compromised for both rice *PI* paralogs, and employed genetic complementation assays to test
80 their functional conservation. These data provide a deeper understanding of the extent of
81 functional divergence between the rice *PI* paralogs. Moreover, we deciphered novel processes
82 regulated by rice *PI* paralogs, such as flowering time, panicle exsertion and ovule development.
83 Importantly, we delineate some gene targets that underlie lodicule development and
84 physiology, and the nonredundant role of OsMADS2 in regulating flowering time. Our data
85 emphasize the importance of investigating homeotic genes outside the core eudicot models to
86 gain novel insights into their evolutionary conservation and diversification.

87 **Results**

88 **OsMADS2 controls floral organ number and flowering time**

89 While the *OsMADS2 dsRN*Ai lines (Prasad and Vijayraghavan, 2003) and mutant reported very
90 recently by Wang and colleagues (2024a) had abnormal lodicules, normal stamen morphology
91 and fertility, Yao and colleagues (2008) described low fertility attributed to poor anther
92 dehiscence. This discrepancy highlights the necessity of in-depth study of developmental
93 phenotypes in several mutant alleles. In this respect, we generated multiple loss-of-function
94 alleles of *OsMADS2* by CRISPR/Cas9 gene editing (Supplementary Fig. S1, A-C). The
95 *osmads2*^{i1}*-dbd* allele with a single base pair (bp) insertion caused a frameshift within the
96 MADS DNA binding domain (DBD), leading to a premature stop codon. The *osmads2*^{i1},
97 *osmads2*^{d2}, and *osmads2*^{d8} alleles contained a 1 bp insertion, a 2 bp deletion, and an 8 bp
98 deletion, respectively and created premature stop codons within the coiled-coil keratin-like
99 domain (K domain) that is involved in oligomerization. Segregation analyses of different
100 *osmads2* alleles in the T4 progeny showed no evidence of segregation distortion from the
101 expected Mendelian ratios (Supplementary Table S1).

102 Morphological characterization of pre-anthesis mature spikelets was performed on
103 homozygotes for all mutant alleles, on biallelic *osmads2*$^{i1/d2}$ and on heterozygous *OsMADS2*$^{+/d8}$
104 plants. For detailed investigation, we focused on *osmads2*$^{d8/d8}$ plants using Scanning Electron
105 Microscopy (SEM) and histological sectioning. Florets from the different homozygous and
106 biallelic mutants consistently exhibited abnormally long lodicules and occasionally displayed
107 increased organ number (Fig. 1B; Supplementary Fig. S2, B-I). The abaxial epidermis of these
108 abnormal lodicules comprised elongated cells that phenocopy cells on the wild-type (WT)

109 marginal tissue of the palea (MTP; Supplementary Fig. S2O). Furthermore, these defective
110 lodicules had reduced thickness and reduced number of vascular bundles (Fig. 1J and
111 Supplementary Fig. S3B). Additionally, we noted instances of cell wall lignification in the
112 mutant lodicule (Fig. 1J) and a transformation of the normally bricklike shaped parenchyma
113 cells that form several internal tissue layers of the wild type lodicule (Fig. 1L) to polygonal
114 cells (Fig. 1M). These mutant phenotypes indicate a partial homeotic transformation of
115 *osmads2* lodicule to MTP which, to a large extent, phenocopy the abnormalities of *OsMADS2*
116 dsRNAi transgenic florets (Prasad and Vijayraghavan, 2003; Yadav et al., 2007), while
117 lodicule phenotype reported in other *osmads2* mutants (Wang et al., 2024a) is not histologically
118 characterized.

119 Unlike lodicules, gross stamen morphology and pollen viability in *osmads2*$^{d8/d8}$ plants, and
120 other *osmads2* alleles, were normal and mutant plants were fully fertile (Fig. 1B;
121 Supplementary Fig. S2M; Supplementary Fig. S3J; Supplementary Fig. S4, B and H), as is also
122 recently reported by Wang et al. (2024a). Rarely, the alleles reported here show lodicule-
123 stamen or stamen-carpel chimeric organs and even partial 'superwoman-like' phenotype, with
124 reduced stamen number and concomitant increase in carpel number (Supplementary Fig. S2,
125 D and H; Supplementary Table S2). The heterozygous *osmads2*$^{+/d8}$ florets were normal though
126 very infrequently (n=2/100) lodicules were mildly elongated and organ number were increased
127 (Supplementary Fig. S2, J and K). These defects in heterozygous florets may arise from
128 stochastic fluctuation in gene expression (Elowitz et al., 2002; Balázsi et al., 2011), the
129 amplitude of which is magnified upon loss of one allele.

130 Although all *osmads2* mutants had similar lodicule phenotypes, we focussed on *osmads2*$^{d8/d8}$
131 for detailed phenotypic and molecular studies. During inflorescence development, the
132 *OsMADS2* transcript level in the *osmads2*$^{d8/d8}$ mutant was reduced by ~ 4-fold (Supplementary
133 Fig. S1D) and OsMADS2 was not detected in panicle nuclear protein lysates on a Western blot
134 using anti-OsMADS2 antibody (Supplementary Fig. S1E). These data confirm that
135 *osmads2*$^{d8/d8}$ is a null mutant. When *osmads2*$^{d8/d8}$ mutants were grown alongside WT plants in
136 a greenhouse, while vegetative growth was equivalent, surprisingly, *osmads2*$^{d8/d8}$ plants
137 commenced the floral transition nearly twelve days earlier than the WT (Fig. 1H). Interestingly,
138 nearly 5% (n = 533) of *osmads2*$^{d8/d8}$ florets exhibited increased inner organ number
139 (Supplementary Table S2), hinting at the possibility of increased cell proliferation or enlarged
140 meristems in *osmads2* florets. Additionally, ectopic lodicules in *osmads2*$^{d8/d8}$ florets were
141 positioned medially, opposite to the lateral lodicules, normally present in WT (Supplementary

142 Fig. S3E). This indicates a previously unknown role of *OsMADS2* in mediating the asymmetric
143 phyllotaxy of second whorl organs. Taken together, the in-depth study of developmental
144 phenotypes of mutant alleles in *osmads2* revealed previously unreported processes regulated
145 by *OsMADS2*, *i.e.* floral organ number and flowering time.

146 **Ubiquitous overexpression of *OsMADS4* complements *osmads2* phenotypes**

147 The two *PI* clade rice paralogs encode proteins that are 81.7% identical and 93.4% similar
148 (Supplementary Fig. S5B). Studies on *OsMADS4*, using knockdown lines, reported some
149 variations with respect to its role in the regulation of lodicule and stamen development (Kang
150 et al. 1998; Yao et al. 2008). Here, we examined *OsMADS4* function employing a specific
151 dsRNAi cassette (Supplementary Fig. S5D). In *OsMADS4 dsRNAi* transgenic line #1 (termed
152 *osmads4kd* hereafter), *OsMADS4* transcript in 2 cm panicles was ~ 7-fold downregulated
153 (Supplementary Fig. S5C). Despite this robust *OsMADS4* downregulation, *osmads4kd* florets
154 were normal and plants were fertile (Fig. 1C; Supplementary Fig. S2M). These findings are
155 consistent with the only report of mutants in *OsMADS4* locus (Wang et al., 2024a).
156 Collectively, the detailed phenotypic characterization of *osmads2* and *osmads4kd* show that
157 rice *PI* paralogs are fully redundant with respect to stamen specification and could contribute
158 to differing extents for lodicule development.

159 To further interrogate this differential contribution, we ubiquitously overexpressed *OsMADS4*
160 in the *osmads2*$^{i/d2}$ mutant. Interestingly, this complemented the different floral phenotypes of
161 *osmads2*, *e.g.*, the abnormal lodicule and the increased floral organ number (Fig. 1D).
162 However, those *osmads2 OsMADS4-OX* transgenics (termed *osm2 OsM4-OX* hereafter)
163 exhibited abnormal, crescent-shaped anthers (Fig. 1D). Histological sections confirmed a
164 normal lodicule vascular pattern (Supplementary Fig. S3H) and revealed unsynchronized and
165 poorly developed anther locules (Supplementary Fig. S3K). Consistent with anther defects,
166 pollen viability and seed set were significantly reduced (Supplementary Fig. S2M;
167 Supplementary Fig. S4, C and H). From this, we conclude that a precisely fine-tuned expression
168 of *OsMADS4* is required for normal anther development.

169 In the T1 generation, we identified segregants lacking the *OsMADS4-OX* transgene, which we
170 refer to as *osmads2 OsMADS4-tg*$^{-}$ (transgene free). As expected, these plants exhibited lodicule
171 abnormalities typical of *osmads2* mutants. We recorded the flowering time of *osmads2*
172 *OsMADS4-tg*$^{-}$ plants and found that they flowered earlier as compared to WT and *osmads2*
173 *OsMADS4-OX* plants, by nearly seven days and ten days, respectively (Supplementary Fig.
174 S6A). These data reiterate the earlier flowering phenotype of *osmads2*$^{d8/d8}$ - in other alleles,

175 *i.e., osmads2*^{i1} and *osmads2*^{d2}, in homozygous or biallelic mutants. Importantly, these results
176 demonstrate that ubiquitous overexpression of *OsMADS4* complemented the *osmads2* early
177 flowering phenotype. Underscoring the contribution of *OsMADS2*, but not *OsMADS4* to
178 flowering time (Supplementary Fig. S6B), is the expression of *OsMADS2* in the vegetative
179 shoot apical meristem (SAM) of wild type 7 days post-germination seedlings, and whose levels
180 are reduced in *osmads2* seedlings (Supplementary Fig. S6C). Further, our analysis of publicly
181 available RNA-Seq data from 6-week-old SAMs of rice (Gómez-Ariza et al., 2019) and 9-day-
182 old SAMs of *Arabidopsis* (Klepikova et al., 2015) showed that *OsMADS2* and *OsMADS16* are
183 expressed in the SAM, while *OsMADS4*, *Arabidopsis PI* and *AP3* are not (Supplementary Fig.
184 S6D). Taken together, these results suggest that *OsMADS2* expression in the SAM prevents a
185 precocious floral transition and identify a diverging, novel function of *OsMADS2* that
186 distinguishes it from *OsMADS4* and *Arabidopsis PI*. Our data on the complementation of
187 different *osmads2* floral phenotypes suggest that the unequal roles of the rice PI paralogs for
188 lodicule development (Yadav et al; 2007; Yao et al., 2008) is likely a consequence of
189 differences in their expression levels and spatial patterns (Yadav et al., 2007) and that they
190 likely encode equivalent proteins.

191 ***OsMADS4* reinforces lodicule function and identity**

192 To understand the redundant contributions of the rice *PI* paralogs in floral development, we
193 generated a double mutant by crossing *osmads4kd* and *osmads2*$^{d8/d8}$ plants. Among the F2
194 plants, derived from F1 of the genotype *osmads2*$^{+/d8}$ *osmads4kd,* we identified *osmads2*$^{d8/d8}$
195 *osmads4kd* plants. Those plants had no discernible vegetative abnormalities, though floral
196 development was severely altered. The lodicules were severely flattened and elongated
197 throughout their proximal-distal axis (Fig. 1, E and F). Consequence of severe lodicule
198 misspecification as a glume-like organ, all florets remained unopened. Based on the severity
199 of the phenotype in third whorl organs, the *osmads2*$^{d8/d8}$ *osmads4kd* F2 and subsequent
200 generation plants were classified into two groups: Florets of group I plants displayed strong
201 superwoman-like phenotype, with all or majority of the stamens being replaced by ectopic
202 carpels (Fig. 1E). Florets from group II displayed a milder superwoman-like phenotype, as all
203 or most of the stamens were present but sterile (Fig. 1F; Supplementary Fig. S4, E-G).
204 Segregation analysis of the *OsMADS4 dsRNAi* transgene across generations indicates that the
205 T-DNA is stably inherited as a single insertion locus (65/89 plants carried the *OsMADS4*
206 *dsRNAi* transgene) which we found integrated in chromosome 8 intergenic region
207 (Supplementary Fig. S7A). Using insertion site-specific PCR, we inferred that group I (average

208 stamen number 2.4) and group II (average stamen number 5.3) phenotypes are associated with
209 the *OsMADS4* dsRNAi transgene being homozygous and hemizygous, respectively
210 (Supplementary Fig. S7, A and B; Supplementary Table S3).

211 Interestingly, in the unopened *osmads2 osmads4kd* florets, the stamen filaments did not
212 elongate (Fig. 1F). Moreover, all *osmads2 osmads4kd* inflorescences were compromised for
213 emergence from the flag leaf sheath (panicle enclosed, Fig. 1G), suggesting poor rachis
214 elongation. Together, the phenotypes of enclosed panicles and poor stamen filament extension
215 suggest a compromised hormone signaling of cell elongation in *osmads2 osmads4kd*
216 inflorescences and florets.

217 We also observed that the inner SL in ~6% *osmads2 osmads4kd* spikelets were overgrown and
218 greenish, a phenotype seen in only 1.5% in *osmads2*$^{d8/d8}$ single mutants (Supplementary Fig.
219 S2L). The identity of the abnormal floral organs in *osmads2 osmads4kd* spikelets were
220 examined by SEM and histological sectioning. Compared to the *osmads2*$^{d8/d8}$ single mutant,
221 *osmads2 osmads4kd* lodicules exhibited more severe abnormalities: the epidermal cells of the
222 basal and distal parts of the malformed lodicules were elongated and midveins were observed
223 along the proximal-distal axis (Supplementary Fig. S2P Supplementary Fig. S3C).
224 Furthermore, the number of vascular bundles and the thickness of the lodicules were drastically
225 reduced, the adaxial side was lined with bubble-shaped cells resembling those normally lining
226 the adaxial lemma/palea surfaces, and importantly lodicule cell walls were lignified (Fig. 1K;
227 Supplementary Fig. S3, C and D). The sterile anthers of *osmads2 osmads4kd* group II florets
228 had underdeveloped locules and a persistent tapetum, which normally undergoes cell death in
229 WT (Supplementary Fig. S3L). Moreover, sections of the abnormally enlarged SL revealed
230 three vascular bundles, suggesting that they acquired a palea-like identity (Supplementary Fig.
231 S3N).

232 Compared to the *osmads2* single mutant, in which only 5.4% of the florets had an increased
233 number of floral organs, ~ 44% of *osmads2*$^{d8/d8}$ *osmads4kd* florets (58/130) had an increased
234 number of inner organs (Fig. 1F; Supplementary Fig. S3, C and D). The increased number of
235 organs was traced to an earlier developmental defect of increased floret meristem size in
236 *osmads2*$^{d8/d8}$ *osmads4kd* florets, as deduced by SEM of young meristems. SEM revealed a
237 slightly enlarged meristem in *osmads2* florets. Notably, the FM size in the *osmads2*$^{d8/d8}$
238 *osmads4kd* florets at spikelet stage Sp6 was evidently larger than that in either WT or *osmads2*
239 florets (Supplementary Fig. S8). The enlarged FM size in *osmads2*$^{d8/d8}$ *osmads4kd* spikelets is
240 reminiscent of the FM enlargement in the *osmads16/spw1* mutant (Yun et al., 2013).

241 Altogether, we conclude that OsMADS4 can partially contribute to the identity of lodicules
242 and fully support stamen development, likely by forming a functional B-class complex in the
243 absence of OsMADS2, in general agreement with other studies (Yoshida et al., 2007; Wang et
244 al., 2024a). Importantly, by silencing *OsMADS4* in the *osmads2*$^{d8/d8}$ null mutant we identify
245 previously unreported roles for these rice *PI* paralogs in rachis elongation, FM size and floral
246 merism.

247 **Rice *PI* paralogs are required for embryo sac development and suppress parthenocarpy**

248 Florets of *osmads2*$^{d8/d8}$ *osmads4kd* lines were male sterile due to either the absence of male
249 organs or the lack of viable pollens (Fig. 1, E and F; Supplementary Fig. S4, E-G). To test the
250 female fertility of these plants, carpels were dusted with WT pollens. Surprisingly, there was a
251 complete failure of seed set from this crossing (Fig. 2A), despite the presence of ovule-like
252 structures within the central carpel and some of the ectopic carpels in *osmads2*$^{d8/d8}$ *osmads4kd*
253 florets (Supplementary Fig. S3, C and D). These data suggest that the sterility of *osmads2*$^{d8/d8}$
254 *osmads4kd* florets is not merely due to defective male organs.

255 A closer inspection of *osmads2*$^{d8/d8}$ *osmads4kd* ovaries from fully mature florets revealed that
256 some of the ovule-like structures, in the fourth whorl central carpels, bear undifferentiated
257 nucellar tissue lacking differentiated embryo sacs (Supplementary Fig. S9, C-E). Other ovule
258 abnormalities included embryo sac degeneration, embryo sac without egg apparatus, embryo
259 sac without female germ unit, embryo sac without antipodal cells, embryo sac without polar
260 nuclei, and embryo sac that lacks antipodal cells and have misplaced polar nuclei (Fig. 2, D-
261 K). Interestingly, a few ovules (n=3/10) of *osmads2*$^{d8/d8}$ *osmads4kd* florets from group II have
262 smaller embryo sacs apparently encompassing the antipodal cells and the female germ unit
263 (Fig. 2C), suggesting they may possess low female fertility or that their infertility arises from
264 defective fertilization or seed/fruit development. RNA in situ hybridization of the rice *PI*
265 paralogs showed localization of *OsMADS2* to the inner ovary walls and the periphery of the
266 developing ovules, and a uniform expression of *OsMADS4* throughout the ovules (Fig. 3),
267 pointing at their contributions to female fertility.

268 Surprisingly, many of the sterile *osmads2*$^{d8/d8}$ *osmads4kd* florets of both groups displayed ovary
269 expansion; a response that is normally triggered by fertilization (Fig. 4, A-C). Eventually, these
270 expanded ovaries shrunk and aborted (Fig. 4D). Closer inspection showed that they lacked
271 endosperms and embryos (Fig. 4, G, I and J), suggesting that fruit development initiated
272 without the formation of the products of double fertilization, a phenomenon referred to as

273 parthenocarpy. Altogether, these results point to previously unreported roles of the rice *PI*
274 paralogs in embryo sac and seed/fruit development.

275 **Mapping genome-wide occupancy of OsMADS2 in developing florets**

276 To shed light onto the mechanistic roles of OsMADS2 as a floral development regulator, we
277 mapped by Chromatin ImmunoPrecipitation followed by deep sequencing (ChIP-Seq) its
278 binding sites, in panicle tissues with florets in a wide range of developmental stages. Peaks of
279 DNA occupancy were called by comparing the enrichment of aligned reads from ChIP over
280 that from a mock immunoprecipitation (IgG). Peaks called from two independent replicates
281 (24,169 and 10,603, respectively) were mapped with respect to transcription start site (TSS) of
282 predicted genes (-3000 to +3000 bp from the TSS). We observed genome-wide pattern of
283 greater enrichment of binding sites proximal to the TSS (Fig. 5A), as reported for other
284 transcription factors, including the *Arabidopsis* Class B *At*PI and *At*AP3 (Kaufmann et al.,
285 2009; Winter et al, 2011; Wuest et al., 2012). We identified 1536 peaks of high confidence that
286 overlapped in the two biological replicates and showed ≥ 2-fold enrichment at a False
287 Discovery Rate (FDR) ≤ 0.05, when compared to the mock IgG. These peaks were assigned to
288 2589 genes and were located in their vicinity up to 4000 bp from either the TSS or the end of
289 the last exon (Supplementary Data Set 1).

290 We used the MEME-ChIP tool from MEME suite (Machanick and Bailey, 2011) to analyse
291 the DNA sequence from the 1536 high confidence peaks and retrieved significantly enriched
292 sequence motifs (e-value ≤ 0.05). These motifs included CGG-repeats
293 (5'GCGGCGGCGGCGRC3'), T-tracks (TTTTYTTTTTTTTYT), G-repeats
294 (5'GSAGVAGVAGSWGGV3'), and CArG-like (5'TATACAAAGTTTGYA3') *cis*-elements
295 (Fig. 5B; Supplementary Fig. S10A). The distribution of these motifs at the OsMADS2 binding
296 regions was further investigated by scanning 400 bp segments from 3000 bp 3' to 3000 bp 5'
297 of the peak midpoint. Our analyses indicated enrichment of these motifs in the 400 bp window
298 of the peak compared to the 400 bp windows from the flanking sequence (Supplementary Fig.
299 S10B). Surprisingly, no canonical CArG-box [5'CC(AT)6GG3'] motifs were retrieved from
300 MEME analyses. Furthermore, our analyses confirmed that canonical CArG motifs are also
301 not enriched in the 400 bp peak regions compared to the flanking sequences (Supplementary
302 Fig. S10B). In *Arabidopsis*, the genomic binding sites for *At*PI/*At*AP3 are enriched for G-boxes
303 (5′-CACGTG-3′) and GA-repeats (5′-GAGAGAGH-3′, Wuest et al., 2012). Our analyses
304 showed that these motifs are also enriched in peak regions compared to the flanking sequences
305 (Supplementary Fig. S10B). Although MADS domain proteins are known to bind to CArG-

306 boxes, they have been shown to bind non-CArG box sequences *in vitro* (Hill et al.,
307 1998). Together, our analyses do not exclude OsMADS2 binding to canonical CArG-boxes,
308 rather our data suggest preferential association to chromatin that are enriched in other motifs
309 including GCC-repeats and CArG-like sequences.

310 To validate the ChIP-Seq results, we tested a number of loci associated with the peaks from
311 our genome-wide analyses by ChIP-qPCR on two independent chromatin preparations. These
312 loci were chosen based on their annotations to genes functionally relevant to *OsMADS2*
313 developmental roles. In panicle tissues of 0.5-1 cm, we validated OsMADS2 binding to
314 *GLYCOSIDE HYDROLASE 9B16* (*GH9B16*), *HEAT STRESS TRANSCRIPTION FACTOR*
315 *C1b* (*HSFC1B*), *PROLIFERATING CELL FACTOR 2* (*PCF2*), *CYCLIN-P4-1-LIKE*,
316 *ETHYLENE RESPONSE FACTOR 61* (*ERF61*) and *PROTEIN TRANSPORTER 2* (*PTR2*, Fig.
317 5). In 1-2 cm inflorescences, we confirmed OsMADS2 binding to *BETA GLUCANASE 1/*
318 (*EGL1,* Supplementary Fig. S10C). The functions of *PCF2* and *CYCLIN-P4-1-LIKE* in cell
319 division can relate to the abnormalities in floral meristem size, organ number, and lodicule
320 shape observed in *osmads2* mutants. *EGL1* and *GH9B16* encode endo-(1,3;1,4)-β-glucanase
321 and glycoside hydrolase, respectively, are proposed to aid the partial hydrolysis of cell wall
322 components to permit turgor-driven cell expansion (Cosgrove et al., 1999; Akiyama et al.,
323 2009; Xie et al., 2013). Hence, these are important direct OsMADS2 target genes that can
324 facilitate normal lodicule function. Similarly, *PTR2* can account for OsMADS2's role in
325 vascular patterning (Li et al., 2015) while, *HSFC1B*, as a target of OsMADS2 (Fig. 5, C and
326 D; Fig. 6B), may contribute to osmotic regulation and lodicule function based on its role in the
327 expression of aquaporins and ion transporters under stress conditions (Schmidt et al., 2012).
328 Together, these results provide insights into the molecular roles of OsMADS2 deciphered from
329 its binding sites in developing rice florets that, point to roles in controlling cell wall elasticity,
330 vascular development, osmotic regulation, and cell proliferation.

331 **Global transcriptome profiling of *osmads2*$^{d8/d8}$**

332 The role of OsMADS2 in the regulation of downstream target gene expression for specific
333 developmental outcomes was studied in the developing panicles by global transcriptome
334 profiling (RNA-Seq), and in the vegetative SAMs *via* RT-qPCR (Fig. 6; Supplementary Data
335 Set 2). In the developing panicles, we compared the transcriptomes of *osmads2*$^{d8/d8}$ and WT
336 across three progressive developmental pools. These pools comprised immature
337 inflorescences: 0.2-0.5 cm (termed early hereafter), 0.5-1 cm (termed middle hereafter), and 1-
338 2 cm (termed late hereafter). The early pool contained florets undergoing meristem

339 specification, organ primordia initiation and patterning, the middle pool comprised florets with
340 differentiating organs, and the late pool had florets undergoing organ growth and early
341 gametogenesis. For each developmental pool, RNA-Seq was performed on two biological
342 replicates of *osmads2*$^{d8/d8}$ and three biological replicates of WT. The high number of
343 differentially expressed genes (DEG) in the "middle pool" (2215 of the total 2550 DEGs across
344 three pools, at fold-change ≥ 2; FDR ≤ 0.05, Supplementary Data Set 2), is consistent with the
345 high *OsMADS2* levels in these tissues (Supplementary Fig. S11A). This implies important roles
346 for *OsMADS2* during organ differentiation. Among the DEGs, more than 82% of genes at any
347 developmental pool were downregulated (Supplementary Fig. S11B), indicating OsMADS2
348 acts majorly as an activator of target gene transcription. Interestingly, in all WT tissue libraries,
349 *OsMADS2* had higher expression levels than *OsMADS4* (Supplementary Fig. S11C), pointing
350 to significant differences in the *cis*-elements driving these paralogous genes.

351 To uncover molecular functions, biological processes, and cellular components controlled by
352 OsMADS2 the DEG datasets were first grouped into those activated or repressed by
353 OsMADS2. Subsequently, gene ontology (GO) enrichment analysis (Fig. 6A; Supplementary
354 Data Set 3) was performed. Several enriched GO terms relate to OsMADS2 roles in lodicule
355 and stamen development. Notable are the terms "water homeostasis" and "response to water
356 deprivation" in the activated DEG subset of the middle tissue pool, the terms "lignan
357 biosynthesis" and "plant type cell wall" in the repressed DEG subsets of the middle and late
358 pools, respectively. These GO terms relate to lodicules as cell wall elasticity and water
359 transport facilitate their rapid swelling during anthesis. Enrichment of the GO term "anther
360 development" in the activated subset of late pool and the term "carpel formation" being
361 enriched in the repressed subset in the middle pool reflect on the stamen development roles for
362 OsMADS2. This is consistent with the homeotic transformation of stamens to ectopic carpels
363 in *osmads2* and *osmads2*$^{d8/d8}$ *osmads4kd* florets. Phytohormones control both cell proliferation
364 and organ differentiation. Remarkably, the term "auxin biosynthetic process" was enriched in
365 the repressed DEG subset in the early pool (Fig. 6A and Supplementary Data Set 3). Possibly
366 the elevated *YUCCA3* (*YUC3*) and *YUC7* expression in *osmads2*$^{d8/d8}$ young florets (Fig. 6B)
367 underlies the increased organ number, given the auxin roles in this process (Krizek, 2011).

368 We present some OsMADS2 downstream targets that are annotated with relevant functions.
369 Given the partial redundancy of *OsMADS2* and *OsMADS4,* we also discuss some biologically
370 relevant DEGs that are affected at lower threshold of transcript fold change (≥ 1.5-fold change
371 regulation at FDR ≤ 0.05) in *osmads2*$^{d8/d8}$. The precocious flowering of *osmads2*$^{d8/d8}$ plants

372 may be linked to lower expression of *OsGIGANTEA* (*OsGI*) and *OsMADS55* in the early
373 inflorescence pool (Fig. 6B; Supplementary Data Set 2). Further interrogation of gene
374 expression revealed steady downregulation of *OsGI* and upregulation of *OsMADS50* in
375 *osmads*$^{d8/d8}$ vegetative SAMs of 30-day, 50-day, and 80-day post germination which also had
376 increased expression (P value = 0.053) of *Early heading date 1* (*Ehd1*, Fig. 6D). These data are
377 consistent with *osmads*$^{d8/d8}$ early flowering and suggest OsMADS2 could contribute to this trait
378 *via* transcriptional regulation of such flowering regulators (Hayama et al., 2003; Doi et al.,
379 2004; Ryu et al., 2009; Lee et al., 2012) during the vegetative growth.

380 The abnormal vasculature patterning in *osmads2* lodicules can be related to the deregulation of
381 *PTR2, HOMEOBOX GENE 1* (*HOX1*), and *ILA1 INTERACTING PROTEIN 3* (*IIP3*, Fig. 6B;
382 Supplementary Data Set 2). These genes have vascular development functions (Scarpella et al.,
383 2000; Ning et al., 2011; Li et al., 2015). Cell wall thickening or lignification in *osmads2*
384 lodicules is consistent with the upregulation *PECTIN METHYLESTERASE 24* (*PME24*) and
385 *BETA GLUCOSIDASE 30* (*BGLU30*) (Fig. 6B; Supplementary Data Set 2). Particularly
386 interesting is the report of PMEs regulating floret opening time by modulating pectin
387 methylesterification in lodicules (Wang et al., 2022). Temporal floret opening is aided by
388 lodicule expansion which is driven by the influx of water, associated with the accumulation of
389 K^+, osmotic solutes such as sugar and di- and tri-peptides, and the increased expression of
390 aquaporins (Heslop-Harrison and Heslop-Harrison, 1996; Choi et al., 2020; Li et al., 2022). In
391 this regard, several DEGs in *osmads2*$^{d8/d8}$ inflorescences encoded K+ channels, *e.g. Two-Pore*
392 *K+ channel b* (*TPKb*, Ahmad et al., 2016), peptide transporter, *e.g. PTR2*, and aquaporins, *e.g.*
393 *TONOPLAST INTRINSIC PROTEIN 4;1* (*TIP4-1*), *TIP4-3*, *PLASMA MEMBRANE*
394 *INTRINSIC PROTEIN 1A* (*PIP1A*). The downregulation of these genes in *osmads2* (Fig. 6B;
395 Supplementary Data Set 2) could compromise osmoregulation and turgor pressure in lodicules,
396 and in turn cause the ever-closed *osmads2*$^{d8/d8}$ *osmads4kd* florets. Notably among the DEGs of
397 the middle pool dataset are *RICE SQUAMOSA PROMOTER-BINDING-LIKE 16* (*SPL16*) and
398 *FLORAL ORGAN NUMBER 1* (*FON1;* Fig. 6B; Supplementary Dataset 2). SPL16 is a positive
399 regulator of cell division (Wang et al., 2012) and its downregulation in *osmads2*$^{d8/d8}$ can relate
400 to the reduced thickness or the reduced pararenchymatous layers in mutant lodicules. The
401 reduced expression of *FON1* aligns with increased organ numbers (Suzaki et al, 2004) in
402 *osmads2* and *osmads2 osmads4kd* florets. Consistent with the conserved functions of *PI*-clade
403 genes for third whorl organ differentiation, several DEGs in *osmads2* inflorescences were
404 implicated in anther and pollen development (Fig. 6B; Supplementary Data Set 2). Examples

are *TAPETUM DEGENERATION RETARDATION* (*TDR*; Li et al., 2006), *SPOROCYTELESS* (*SPL*; Ren et al., 2018) and *MICROSPORE AND TAPETUM REGULATOR1* (*MTR1*; Tan et al., 2012). Some DEGs in *osmads2* inflorescences may underlie the compromised panicle exsertion seen in *osmads2 osmads4kd* plants. Among these are *EPIGENETIC SHORT PANICLE* (*ESP*), encoding a long noncoding RNA implicated in panicle length (Luan et al., 2019) and the gibberellic acid (GA) biosynthetic genes *GA20ox4* and *GA3ox2* (Fig. 6B; Supplementary Data Set 2).

The exacerbation of lodicule malformation and manifestation of other abnormal phenotypes in *osmads2 osmads4kd* plants, that are neither seen in *osmads2* nor in *osmads4kd* point at other target genes redundantly controlled by both PI-like factors. Towards this end, we curated from the literature functionally relevant genes and interrogated their expression levels in the doubly perturbed *osmads2 osmads4kd* inflorescences (Fig. 6C). For some of the tested genes, *i.e., Cyclin D2-2* (*CycD2-2*), *OPEN GLUME1* (*OG1*) and *MALE STERILITY 2* (*MS2*) differential expression, at a stringent at 2-fold cutoff, was not seen. Importantly, other genes were deregulated at this cutoff and this is consistent with the floral phenotypes observed in *osmads2 osmads4kd*. Among these are *DIURNAL FLOWER OPENING TIME 1* (*DFOT*), involved in lodicule development (Wang et al., 2022), *HOMEOBOX GENE 12* (*HOX12*), involved in panicle enclosure (Gao et al., 2016), *KIP-RELATED PROTEIN 3* (*KRP3*) regulating cell cycle (Mizutani et al., 2010), and auxin biosynthetic genes *YUC1* and *TRYPTOPHAN DEFICIENT DWARF 1*/*TDD1* (Sazuka et al., 2009). Additionally, *MADS13*, a Class D gene (Dreni et al., 2007) had elevated expression in *osmads2 osmads4kd*. However, it is uncertain whether this contributes to the defective ovule development or the excessive ovule proliferation. The auxin biosynthetic gene *NITRILASE 1/NIT1* (Abu-Zaitoon, 2024), the aquaporin *TONOPLAST INTRINSIC PROTEIN 4-1/TIP4-1* and the JAZ6 and JAZ7 encoding Jasmonate ZIM-domain proteins implicated in lodicule development (Cao et al., 2021; Wang et al., 2024b) are examples of genes bound by OsMADS2 (Supplementary Data Set 1) and deregulated in *osmads2 osmads4kd* florets.

The distinct roles of OsMADS2, as compared to *At*PI, suggest significant changes in their downstream targets. We thus compared the DEG datasets in *pi-1* (Wuest et al., 2012) with those in *osmads2*$^{d8/d8}$. Orthologous group analysis indicates nearly 15% of *OsMADS2* downstream targets have orthologs that are deregulated in at least one floral developmental stage of *Arabidopsis pi-1* inflorescence (Supplementary Data Set 4). Examples of such conserved gene targets are *Oryza sativa HOMEOBOX 1* (*OsHOX1*), *Carbon Starved Anther*

438 (*CSA*), and *BASIC HELIX-LOOP-HELIX PROTEIN 120* (*BHLH120*). *BHLH120* and its
439 *Arabidopsis* orthologs *HEC1* and *HEC2* were upregulated in the *osmads2*$^{d8/d8}$ and *pi-1* DEG
440 datasets, respectively. The elevated expression of *HEC* orthologs in *pi* mutants suggest that the
441 suppression of carpel development regulators by B-function genes may be evolutionarily
442 conserved. Remarkably, the orthologs of several rice TCP transcription factor genes which are
443 targets of OsMADS2 were also represented in *pi-1* DEG dataset. Examples are *OsPCF1*,
444 *OsPCF5*, *OsTCP9*, and *OsTCP21*. Notably, orthologs of OsMADS2 downstream targets
445 regulating flowering time *e.g. GI* and *MADS55*, and orthologs of the auxin biosynthetic genes
446 *YUC3* and *YUC7*, were not reported in the *pi-1* DEG dataset. Taken together, these analyses
447 provide clues to some evolutionary conserved or divergent functions of *OsMADS2* as compared
448 to *AtPI*.

449 **OsMADS2 direct targets relevant to lodicule development and physiology have enhanced**
450 **expression in the developing lodicules**

451 Nearly 11% of the differentially expressed genes (1.5-fold, FDR ≤ 0.05) from all the three
452 RNA-Seq data sets (Supplementary Fig. S11D), occur in the OsMADS2 ChIP-Seq data set,
453 identifying them as direct gene targets. Yet other DEGs we propose can be regulated by
454 transcription factors that are directly regulated by OsMADS2. We constructed OsMADS2
455 centric gene regulatory networks (GRNs) that link to certain target genes encoding OsMADS2
456 transcription factor targets in the early and middle tissue pools (Supplementary Fig. S12;
457 Supplementary Fig. S13; Supplementary Data Set 5). OsMADS2 binding and regulation of
458 some of genes in these GRNs were validated by ChIP-qPCR and RT-qPCR (Fig. 5C; Fig. 6, B
459 and C). Further we present a small OsMADS2 centric GRN (Fig. 6E) that links to target genes
460 implicated for cell division control, osmotic homeostasis, vascular development and other
461 organ differentiation functions that are disrupted in either *osmads2* or *osmads2 osmads4kd*
462 panicles.

463 The expression profile of some of these genes in wildtype mature floral organs was analysed
464 by RT-qPCR (Fig. 7A; Supplementary Fig. S14A). We find enriched RNA levels in lodicules
465 of pre-anthesis florets for *PIP1A*, *PTR2*, *CYCLINE-P4*-1-LIKE, *PCF2*, *GH9B16*, *HSFC1B*,
466 *TPKb*. Additionally, the spatial temporal expression profile by RNA *in situ* hybridization
467 showed that the transcripts for the direct target genes encoding aquaporin (*PIP1A*), peptide
468 transporter (PTR2), and *CYCLINE-P4*-1-LIKE are abundant during lodicule organogenesis
469 (Fig. 7B-S).

470 Given the large number of cell cycle regulators, as direct and indirect targets of OsMADS2,
471 and the floral or lodicule phenotypes of *osmads2 osmads4kd*, we examined cell proliferation
472 by EdU labelling assay. We compared the number and distribution of cells in S phase in WT
473 and *osmads2 osmads4kd* florets. The data uncovered that the number of S-phase cells per unit
474 area in inner floral organs is significantly higher in *osmads2 osmads4kd* florets (Fig. 7T-V).
475 We further interrogated the spatial distribution of S-phase cells in the lodicule body (LoB) and
476 lodicule tip (LoT), two regions of the lodicule that are identified by differences in the abaxial
477 epidermal cell width and in the number of their inner cell layers (Supplementary Fig. S14B).
478 These data demonstrated significant reduction in the number of S-phase cells in *osmads2*
479 *osmads4kd* LoB, concomitant with increased number of S-phase cells in the LoT (Fig. 7W-X).
480 This points at striking change in the spatial cell division of the abnormally flattened and
481 apically elongated *osmads2 osmads4kd* lodicules as compared to the fleshy WT lodicules.
482 Given failure of floret opening in *osmads2 osmads4kd* florets and the finding that a large
483 number of direct and indirect OsMADS2 targets encode aquaporins and osmotic regulators, we
484 determined the osmolality of cell saps from lodicules of WT and *osmads2 osmads4kd* pre-
485 anthesis florets. Sap from *osmads2*$^{d8/d8}$ and *osmads2 osmads4kd* abnormal lodicule exhibited
486 significantly reduced osmolality as compared to WT (Fig. 7Y). These data suggest that the
487 failed opening of these mutant florets could arise from the defective lodicule physiology.

488 **Discussion**

489 **Basis of divergence and novel Class B functions for the rice *PI* paralogs**

490 In this study, we showed that *osmads2* null mutants have abnormal lodicules but unaffected
491 stamens, while *osmads4kd* plants have normal florets as is reported by Yao and colleagues
492 (2008) and also in a very recent report of mutants in *OsMADS4* (Wang et al., 2024a). Together,
493 these data demonstrate that compared to stamen, lodicule development is more sensitive to loss
494 of function or reduction in PI activity and suggest divergence of the rice *PI* paralogs for lodicule
495 development. These studies also reinforce redundant contributions from OsMADS4 for
496 lodicule development are apparent in the context of *osmads2* loss-of-function, as *osmads2*$^{d8/d8}$
497 *osmads4kd* florets have more severe derangement of lodicule development. Interestingly, no
498 organ-specific sub-functionalization neither redundancy of the maize *PI* paralogs, *Zmm16/Sts1*
499 and *Zmm18/29*, are reported, since *sts1* mutants have a homeotic conversion of both lodicules
500 and stamens into palea-like organs (Bartlett et al., 2015). Moreover, the rice *PI* paralogs display
501 expression differences that may underlie functional divergence, since *OsMADS2* RNA levels
502 are higher than those of *OsMADS4* (Supplementary Fig. S11D) in all developing panicle pools

503 tested here. Furthermore, differences in expression patterns and abundance in floral organs is
504 apparent in RNA *in situ* hybridization data (Yadav et al., 2007; Fig. 3). Additionally,
505 *OsMADS2*, but not *OsMADS4* is expressed in the vegetative SAM. This we indicate is
506 functionally relevant as we find early flowering in *osmads2*$^{d8/d8}$ and normal flowering in
507 *osmads4kd* plants. This role for rice *OsMADS2* in flowering time represents a novel function
508 for a cereal Class B gene. Recently, Shi and colleagues (2024) reported the interaction of
509 daylily PI and AP3 with the flowering suppressor TERMINAL FLOWER 1, in yeast, and their
510 overexpression advance flowering time in *Arabidopsis*, suggesting that Class B MADS factors
511 from other monocot species could also regulate flowering time.

512 Unlike the lodicule, stamen development is, fully, redundantly controlled by the two rice PI
513 paralogs, since *osmads2* and *osmads4kd* florets have normal stamens as is also seen in various
514 knockdown lines and the recently reported *osmads4* mutants (Yadav et al., 2007; Yao et al.,
515 2008; Wang et al., 2024). However, we report, for the first time, that homeotic conversion of
516 stamen to carpel, in *osmads2 osmads4kd* florets, is associated with the copy number for
517 *OsMADS4* dsRNAi transgene, suggesting that stamen development in *osmads2* mutant is
518 sensitive to the dosage of OsMADS4 activity. By crossing *osmads2*$^{d8/d8}$ with *osmads4kd*, we
519 generated stable and fertile *osmads2*$^{d8/+}$ *osmads4kd* with a hemizygous single insertion of T-
520 DNA for *OsMADS4* knockdown. This line we exploited as a valuable genetic stock to identify
521 double mutant *osmads2*$^{d8/d8}$ *osmads4kd* segregants over generations, for in depth
522 characterization. In these plants we identified phenotypes, not seen in the single mutant parents
523 of the cross. Thus, we uncover panicle exsertion and suppression of parthenocarpy as novel
524 functions redundantly controlled by the rice PI paralogs. Both are essential physiological
525 processes that ensure high quality grain yield in rice. Panicle enclosure, is a distinctive
526 phenotype seen in nearly all male-sterile rice lines (Liang et al., 2008). It also triggers water
527 stress induced sterility and impair effective pollination, leading to low seed setting (O'Toole
528 and Namuco, 1983). Parthenocarpy, fruit formation from maternal tissue without fertilization,
529 adversely affects reproductive success. Plants evolved several mechanisms by which they
530 counteract this process (reviewed in Joldersma and Liu, 2018). While we show that rice *PI*
531 paralogs redundantly suppress this process (Fig. 8), we point that this could be a conserved
532 function or an example of convergent evolution for B-class activity, as loss of function in PI
533 and AP3 orthologs triggers parthenocarpy in other dicot species, *e.g.* tomato and apple (Yao et
534 al., 2001; Li et al., 2024).

535 **Conserved functions of the rice PI paralogs**

536 Expectedly *osmads2* and *osmads2 osmads4kd* florets had abnormal lodicules and stamens,
537 consistent with the conserved requirement for B-Class function for second and third whorls
538 organ development. However, these mutants also exhibited other abnormalities not reported in
539 studies on these rice *PI* – clade genes. Some of these phenotypes we uncovered are similar to
540 developmental defects reported in some mutants in *PI* – clade genes from other species. Many
541 *osmads2* and *osmads2 osmads4kd* florets had increased stamen organ number, a phenotype
542 seen in the maize *sterile tassel silky ear1* (*sts1*) mutant but not seen in the *Arabidopsis pi-1*
543 mutant (Bowman et al., 1989; Yang et al., 2003; Bartlett et al., 2015). However, the increased
544 second whorl organ number of *osmads2* florets (Fig. 1B) is not observed in the maize *sts1*
545 mutant (Bartlett et al., 2015). Interestingly, in *Nigella damascene*, a dicot species with spiral
546 not whorled flowers, an AP3 paralog influenced perianth organ number (Gonçalves et al.,
547 2013). This observation hints at the likelihood of MADS-box class B genes having a role in
548 the control of floral organ number in diverse species. Furthermore, the emergence of ectopic
549 medial lodicules in *osmads2* mutant restores a whorl of primordia in the second whorl and
550 indicates *OsMADS2* contributes to positional lodicule asymmetry, possibly through
551 asymmetric expression in the second whorl as observed for its maize ortholog, *Sts1* (Bartlett et
552 al., 2015).

553 Unexpectedly, *osmads2 osmads4kd* were female sterile and displayed varying abnormal ovule
554 differentiation. Although the *Arabidopsis pi* and *ap3* mutants are female fertile (Krizek and
555 Meyerowitz, 1996), mutants in the rice and barley *AP3* homologs, *OsMADS16* and *HvMADS16*
556 (Nagasawa et al., 2003; Selva et al., 2023), are female sterile. While this suggests a conserved
557 female fertility role for class B MADS factors from two related cereal species, the fertile maize
558 *Si1* and *Sts1* mutants (Ambrose et al., 2000; Bartlett et al., 2015), indicate important rice-maize
559 and barely-maize divergences in B-class activity.

560 The identity of floral organs is dictated by the combinatory functions of different classes of
561 MADS domain transcription factors (Coen and Meyerowitz, 1991; Favaro et al., 2003;
562 Pinyopich et al., 2003). In *Arabidopsis*, although ectopic expression of either *PI* or *AP3* alone
563 does not significantly alter flower development (Jack et al., 1994; Krizek and Meyerowitz,
564 1996), their simultaneous ectopic expression converted sepals to petals, and carpels to stamens
565 (Krizek and Meyerowitz, 1996). In rice, ectopic overexpression of *OsMADS16* enhanced
566 *OsMADS4* expression and produced multiple stamen-like structures in the fourth whorl (Lee et
567 al., 2003). Interestingly, in our study, ubiquitous overexpression of *OsMADS4* in *osmads2*

568 mutants did not trigger homeotic transformations of floral organs. This indicates that the
569 coexistence of PI and AP3 homologs, at appropriate levels, is a conserved prerequisite for
570 ectopic B-class activity in rice and *Arabidopsis*. Importantly, we have shown that ubiquitous
571 overexpression of the rice *PI* paralog *OsMADS4* led to underdeveloped stamens, a phenotype
572 observed on overexpression of *OsMADS16*, the *AP3* homolog, in rice (Lee et al., 2003). Taken
573 together, these data suggest that excessive, ubiquitous B-class activity is detrimental to normal
574 rice anther development.

575 **Gene targets of the rice PI paralog, OsMADS2**

576 The genome-wide binding sites and target genes of OsMADS2 identified here reveal its direct
577 and indirect control of the expression of ~2500 genes that can be assigned to different
578 functional categories. Enrichment of GO terms "sequence-specific DNA-binding" and
579 "transcription factor activity" in the DEG datasets of the early and middle pools
580 (Supplementary Data Set 3), imply that during early floret development, OsMADS2 mediates
581 organ formation, largely by controlling the expression of genes encoding transcriptional
582 regulators. Whereas, during later stages of floret development, it acts more directly on target
583 genes with fewer genes encoding downstream transcription factors, as has been also suggested
584 for the *Arabidopsis* PI/AP3 (Wuest et al., 2012). This is consistent with 3.5% DEGs (1.5-fold,
585 FDR ≤ 0.05) are bound by OsMADS2 from the late RNA-Seq data set as compared to 6.6%
586 and 11% from the early and middle RNA-seq data sets, respectively (Supplementary Fig.
587 S11D). Like seen for the *Arabidopsis pi-1* (Wuest et al., 2012), the number of DEGs in *osmads2*
588 inflorescences increased with progressive flower development, specifically when we compare
589 the early and middle DEG data sets. However, in the late data set, the number of DEGs sharply
590 reduced which could be attributed to the increased heterogeneity of developing tissues in the
591 late pool as it constitutes inflorescences ranging from 1 to 2 cm. Thus, we speculate that the
592 actual number of genes regulated by OsMADS2 activity in late-stage data set may also
593 presumably be similar to that of the middle data set.

594 The large number direct and indirect OsMADS2 targets imply it participates in the regulation
595 of many pathways required for floral organ initiation and differentiation, consistent with
596 phenotypes seen in *osmads2* and *osmads2 osmads4kd* plants. The negative regulation of the
597 auxin biosynthetic genes *YUC3* and *YUC7* in the early developmental pool leads us to speculate
598 that local auxin levels contribute to the control of floral organ number and the asymmetrical
599 lodicule positioning. However, other organ phenotypes such as the excessive growth of ovule
600 nucellar tissues and the parthenocarpy in the *osmads2 osmads4kd* florets suggest rice PI

601 paralogs dynamically regulate auxin biosynthesis and transport during later stages of floral
602 organ development. As a regulator of lodicule development, OsMADS2 controls the
603 expression of many genes associated with cell wall modification, e.g. *PME24* and *BGLU30*
604 and several *EXPANSINS* (Supplementary Data Set 3). In various studies, the opening time of
605 rice florets was altered by manipulating cell wall characteristics through *PME40, PME42,* and
606 *BETA-1,3-GLUCANASE 4* (*GNS4*, Wang et al., 2022; Xu et al., 2022). Therefore, the
607 OsMADS2 targets (*PME40, PME42* and *BLGU30*) offer promising future screens for
608 cleistogamy florets and/or for lines with advanced floret opening time. Such traits would
609 facilitate breeding and mitigate heat-induced floret sterility. Modulation of genes for cell wall
610 characteristics is associated with response to drought, as inferred from different omics data sets
611 (reviewed in Veronico et al., 2022). In this context, it is worth noting that OsMADS2 regulates
612 many genes associated with response to water stress (Supplementary Data Set 3). Such genes
613 along with other targets involved in cell wall metabolism and the transport of K^+ and osmotic
614 solutes, may collectively facilitate lodicule function. From these categories, we interrogated
615 the expression of various direct targets: *GH9B16*, *PME24*, *PIP1A*, *PTR2* and *TPKb*, and
616 showed their enrichment expression in lodicules. The floret opening mediated by lodicule
617 expansion coincides with stamen filament elongation. Like reported by Zhao and colleagues
618 (2022), stamen filaments also failed to elongate in the unopened *osmads2*$^{d8/d8}$ *osmads4kd* floret
619 (Fig. 4B). This together suggest common triggers for cell expansion in lodicule and stamen
620 filaments. The activity of these genes, as they enable cell wall loosening, water influx and cell
621 expansion, may control these timely synchronised processes.

622 Although OsMADS2 targets constituted genes encoding various transcription factor families,
623 the MADS-box gene family, despite being represented in the ChIP-Seq data set, were depleted
624 from the three progressive DEG data sets (2-fold change; FDR $\leq$ 0.05) This implies that
625 OsMADS2 could be regulating other MADS-box genes redundantly with other factors, *i.e.*
626 OsMADS4 and OsMADS16. Given the physical interaction of OsMADS2 and
627 OsMADS32/CFO1 (Wang et al. 2015), and that *OsMADS2* levels are normal in *cfo1* (Hu et al.
628 2021), the shared phenotypes (abnormal lodicules and chimeric floral organs) of *osmads2* and
629 *cfo1*, imply that OsMADS2 and OsMADS32 function in a complex to regulate lodicule
630 development and floral organ identity. In conclusion, the target genes of OsMADS2 unravelled
631 in this study provide new insights into the mechanistic role of *OsMADS2* in rice floral
632 development (Fig. 8). Importantly, stable and fertile *osmads2* mutants and the doubly

633 perturbated *osmads2*$^{d8/+}$ *osmads4kd* plants will enable future genetic and gene regulatory
634 studies on the temporal and spatial control of tissue differentiation in floral organs.

635

636 **Materials and Methods**

637 **Plasmid construction and plant transformation**

638 For CRISPR/Cas9 gene editing of *OsMADS2*, two pairs of primers were designed for
639 respective sets of 20 nucleotide guide RNAs (gRNAs). The first pair of primers (a and b) were
640 annealed and cloned into the commercial pRGEB31 vector to construct a binary vector used to
641 transform rice plants with intended editing in the OsMADS2 DNA-binding domain (designated
642 gRNA1). The second pair of primers (c and d) were annealed and cloned similarly, and the
643 construct was used to generate transgenic plants with intended editing in OsMADS2 K-domain
644 (designated gRNA2). The sequences for the different oligos are given in Supplementary Table
645 S4. For *OsMADS4* dsRNAi-based knockdown, a 290 bp specific fragment (from +1794 to
646 +2083 of the *OsMADS4* genomic locus) was amplified using primers *OsMADS4* FP and
647 *OsMADS4* RP (Supplementary Table 4). This fragment was then cloned into pBluescript in
648 opposite orientations separated by a linker. The generated clone was verified by restriction
649 digestion and Sanger sequencing. Subsequently, the insert in recombinant pBluescript was
650 released and cloned into the binary rice expression vector pUN (Prasad et al., 2001),
651 downstream to the maize ubiquitin promoter (*pZmUbi*), to express the *OsMADS4* hairpin RNA.
652 For overexpression of *OsMADS4* in the *osmads2* mutant background, the *OsMADS4* cDNA
653 was amplified with primers *OsMADS4* CDS FP and RP (Supplementary Table S4), from cDNA
654 transcribed from TP309 panicle tissue RNA, and cloned into pBluescript. A clone verified by
655 restriction digestion and Sanger sequencing was used to release *OsMADS4* cDNA, which was
656 subsequently cloned downstream of the *pZmUbi* into a modified pCAMBIA3300 vector with
657 a *pZmUbi* promotor and a *Nos* terminator. This Basta resistant vector was used to transform
658 rice calli generated from mature seeds of *osmads2* mutant. Binary vectors were mobilized into
659 the LBA4404 *Agrobacterium tumefaciens* strain, which was used to transform WT rice (*Oryza*
660 *sativa* var. Japonica) TP309 embryogenic calli and transgenic lines were raised as described by
661 Prasad et al. (2001). Plants were grown as reported by Prakash et al. (2022). For raising anti-
662 OsMADS2 antibody, a gene-specific *OsMADS2* cDNA fragment encoding the amino acids
663 112 to 209 was cloned into pET-15b and the His-tagged protein was expressed in bacteria
664 grown with 0.5 mm isopropylthio-β-galactoside at 37°C for 3 hours. The His-tagged
665 OsMADS2 partial protein was purified by nickel-nitrilotriacetic acid agarose chromatography,

666 followed by the removal of the His tags by thrombin cleavage. The purified proteins were used
667 to raise rabbit polyclonal antibodies that were affinity purified using the antigen. The
668 specificity of the purified antibody was established by Western blots on nuclear proteins from
669 panicles (Supplementary Fig. S1E).

670 **Genotyping of CRISPR/Cas9 edited *OsMADS2* lines**

671 Genomic DNA regions flanking the editing sites were PCR-amplified using primers *OsMADS2*
672 E3-I3 FP and *OsMADS2* IV RP (Supplementary Table 3). The PCR amplicon was digested
673 with *Sac*I to identify putative edits in *OsMADS2*. Subsequently, the PCR amplicon from
674 putatively edited plants was cloned into *Eco*RV site of pBluescript and at least two pBSKS
675 clones were given for Sanger sequencing to identify the exact edits. To identify plants that had
676 transmissible edits in the germline, independent genotyping was done for two subsequent
677 leaves of the same plant and across different generations. Once mutant plants with stably
678 inherited alleles were identified, Sanger sequencing of PCR products was utilized for further
679 genotyping in advanced generations.

680 **Amplifying the genomic DNA flanking the T-DNA integration site**

681 Restriction Site Extension PCR (Ji and Braam, 2010) was utilized to amplify the genomic DNA
682 flanking the T-DNA harbouring the *OsMADS4* dsRNAi cassette. Briefly, primers p1300 5.0
683 and p1300 5.1, specific to the pCAMBIA1300 left border (Supplementary Table 3), were used
684 to perform the primary and secondary PCRs, respectively. Two amplicons of ~ 1.2 and ~ 1.4
685 kb were obtained from genomic DNA digested with *Sac*I and *Kpn*I, respectively. These
686 amplicons were gel-purified and Sanger sequenced. The genomic sequence flanking the T-
687 DNA left border was then mapped to the rice genome using blastn. To screen transgenic plants
688 for hemi- or homozygosity with respect to the *OsMADS4* dsRNAi cassette, two primers (*OsM4*
689 ds IS FP and RP; Supplementary Table 3) flanking the insertion site were designed and utilized
690 to amplify the WT genomic sequence from the hemizygous segregants.

691 **Phenotypic Characterization**

692 Freshly collected pre-anthesis mature spikelets were examined and photographed using a Leica
693 Wild M3Z stereomicroscope fitted with digital camera (Canon Powershot G5). Pollens from
694 rice anthers at anthesis were stained with either iodine potassium iodide (I_2KI) or 4′,6-
695 diamidino-2-phenylindole (DAPI) for 1-5 mins on a microscope slide and examined under the
696 microscope. Phenotyping of ovaries and ovules by whole-mount eosin B-staining confocal
697 laser scanning microscopy was done according to Zeng and colleagues (Zeng et al., 2007). For
698 SEM, fresh spikelet and inflorescence samples were fixed in 0.1 M sodium phosphate buffer

699 at pH 7.0 containing 3% glutraldehyde (Sigma-Aldrich, St. Louis, USA) for 12-24 hrs. Tissue
700 samples were then post-fixed in 1% osmium tetroxide for 24-48 hrs or until performing the
701 next step. Next, tissue samples underwent graded ethanol dehydration and critical point drying
702 using Pelco CPD2 (Ted Pella, California, USA). Critical point dried samples were mounted on
703 an SEM stub, using double stick conductive carbon tape, sputter coated, and examined. An
704 Ultra 55 FE-SEM with EDS instrument (Carl Zeiss, Oberkochen, Germany) was used for
705 imaging with help from the technician in charge at the Centre for Nano Science and
706 Engineering (CeNSE) at IISc. For histological analysis, tissues were fixed in FAA solution
707 (10% Formalin, 5% Glacial Acetic Acid, 50% Ethanol), dehydrated in an ethanol series, and
708 embedded in paraffin. Sections of 8 um were stained with 0.5% toluidene blue (FisherBiotech,
709 Massachusetts, USA).

710 For 5-ethynyl-2'-deoxyuridine (EdU) labelling, Click-iT® EdU Alexa Fluor® 488 Imaging Kit
711 (ThermoFisher, C10337) was utilized. Panicle tissues of 0.7 cm length were excised and placed
712 in 25 µM EdU solution made in half strength MS (Murashige and Skoog) for 2 hrs, then fixed
713 and embedded in paraffin as described above. Sections of 8 um were dewaxed and processed
714 for detection according to the manufacturer's instructions. Sections from WT and *osmads2*$^{d8/d8}$
715 *osmads4kd* florets of equivalent developmental stage (having roughly equal dimensions) were
716 imaged with Zeiss 710 confocal microscope. Number of S-phase cells in the inner floral organs
717 or in the lodicule were counted manually across all sections of a single floret. The area of the
718 inner floral organs, the area of the tip of the lodicule and the area of the body of the lodicule
719 across all sections of a single floret were measured in FiJi (ImageJ). The number of S-phase
720 cells per unit area in the inner organs were plotted and statistically analyzed for 4 WT florets
721 and 5 *osmads2 osmads4kd* florets, while in case of lodicule the N was equal to 3. For measuring
722 the osmolality of the sap from the lodicules, nearly 80 pairs of lodicules, per biological
723 replicate, were dissected from pre-anthesis florets collected between 09:00-11:00 am.
724 Lodicules were then crushed in a 1.5 ml microcentrifuge tube with an autoclaved micro-pestle,
725 followed by a quick spin at 6000g. The sap was then collected and the osmolality was measured
726 with a vapour pressure osmometer (Vapro5600, Wescor). Three biological replicates of
727 *osmads2*$^{d8/d8}$ and *osmads2*$^{d8/d8}$ *osmads4kd* lodicules were plotted and compared to five
728 replicates of WT.

729 **Western Blotting**

730 Nuclear proteins were isolated according to Busk and Pagès (1997). Protein concentration was
731 estimated by the Bradford method according to the manufacturer's instructions (Sigma Aldrich,

732 Missouri, USA). The protein was separated on an SDS PAGE gel of 12% and transferred to
733 PVDF membrane with a 0.5 µm pore size through Trans-Blot® SD semi-dry transfer cell (Bio-
734 Rad, USA). Blocking was done for 1 hr, followed by incubation with the primary antibody
735 (polyclonal affinity-purified primary antibody against the 11.44 kDa C-terminal region of
736 OsMADS2) for 12 hrs. Washing was done for 3X for 5 min, after which the membrane was
737 incubated with an HRP-conjugated secondary antibody for 1 hr. The membrane was then
738 washed 3X for 5 min each and developed using the Immobilon Forte Western HRP Substrate
739 (Cat# WBLUF0100, Millipore, USA). Images were acquired using an ImageQuant LAS4000
740 Chemidoc instrument (GE HealthCare Bio-Sciences AB, Japan) of the Microbiology and Cell
741 Biology Department at IISc.

742 **ChIP-sequencing, read alignment, peak calling, and gene assignment**

743 Wild-type TP309 panicles were used for the ChIP. The tissue pool ~200mg constituted 4
744 panicles (x) 0.3cm, 4x 0.4cm, 3x 0.5cm, 1x 0.6cm, 1x 0.7cm,1x 0.8cm, 1x 0.9cm, 1x 1cm, 1x
745 1.5cm and 1x 2cm. The tissues were fixed with 1% formaldehyde in a fixation buffer.
746 OsMADS2 ChIP was performed using SimpleChIP® Enzymatic Chromatin IP Kit (Cat #9002,
747 CST, Massachusetts, USA). MNaseI based chromatin was prepared with DNA fragments
748 ranging from 150bp to 900bp. For the ChIP, 8µg of chromatin was used and incubated with
749 6µg of affinity-purified anti-OsMADS2 antibody. The DNA-protein complexes were pulled
750 down using protein-A magnetic beads. Simultaneously, a negative control sample using rabbit
751 IgG antibody (mock IP) instead of the anti-OsMADS2 antibody was processed in the same
752 way. Immunoprecipitated DNA was eluted using the elution buffer provided in the kit and
753 reverse cross-linked using 2M RNase A and 4M proteinase K in 5M NaCl for 6 hours at 65˚C.
754 Reverse-crosslinked ChIP DNA was purified using the phenol/chloroform purification and
755 precipitation method. Approximately 6 ng of ChIP DNA was processed to prepare a library for
756 NGS by using the Kapa kit (Roche, Basel, Switzerland) following the manufacturer's
757 instruction with one modification: library amplification was performed before the double-size
758 selection. NGS was performed using the Illumina HiSeq2500 machine at the Functional
759 Genomics Center Zurich. Sequencing depth ranged from 22 million to 39 million single-end
760 reads per sample. Raw fastq files were processed with FASTQC and Fastp for filtering low
761 quality reads and adaptor trimming. Next, short read alignment was performed by bowtie2
762 version 2.3.5.1 using MSU-TIGR v7 as the reference genome. The bam files with alignment
763 information were process with SAMBAMBA (0.6.6) for sorting and filtering uniquely mapped
764 reads. For peak calling, the uniquely mapped reads were processed with MACS2 (version 2.2.6;

765 Zhang et al., 2008) using the default parameters, keep-dup parameter as AUTO, and effective
766 genome size of 3.50e+08. Briefly, two biological replicates (B5 and B6) of IP and Mock-IP
767 were used. First, peaks from IP B5 were retrieved using Mock-IP B5 as a control. Another set
768 of peaks from IP B5 were retrieved using Mock-IP B6 as a control. Next, peaks from IP B6
769 were recovered using Mock-IP B6 as a control. To determine confident peaks from B5 IP,
770 overlapping peaks from IP B5 over Mock-IP B5 and IP B5 over Mock-IP B6 were recovered
771 and merged. These confident peaks from IP B5 were then merged with overlapping peaks from
772 IP B6. These overlapping, merged peaks from IP B5 and IP B6 were designated as peaks of
773 high confidence. Next, these peaks were assigned to genes in their neighbourhood up to 4000
774 bp from either the start or end of the gene. Finding overlapping peaks and assignment of peaks
775 to genes were performed in R studio using the ChIPpeakAnno library (Zhu et al., 2010)
776 functions, findOverlapsOfPeaks and annoPeaks, respectively. For annoPeaks function,
777 bindingType and bindingRegion were set to "fullRange" and to -4000 and +4000, respectively.
778 Peak distribution with respect to TSS and 3000 bp flanking regions was performed with
779 plotAvgProf from the ChIPseeker Bioconductor package (Yu et al., 2015), using coordinates
780 from "Oryza_sativa.IRGSP-1.0.53.gtf.gz".

781 **ChIP-Seq motif analyses**

782 Coordinates of the confident peaks were defined from IP B5. The midpoints of these peaks
783 were determined and a set of 500 bp (-250 to 249 from the midpoint) sequences was extracted.
784 In these 500 bp sequences, the repeats were masked using RepeatMasker
785 (https://www.repeatmasker.org/) and then submitted to MEME-ChIP from the MEME suite
786 (Machanick and Bailey, 2011). From MEME analyses, we retrieved significantly enriched
787 motifs with E-values ≤ 0.05. Analysis of motif distribution in peak regions and flanking 3000
788 bp at 400 bp windows utilized the R function vmatchPattern from the Biostrings Bioconductor
789 package (Pagès et al., 2022).

790 **RNA-Sequencing and orthologous group analysis**

791 RNA-sequencing was performed for three progressive panicle pools, named early, middle and
792 late. The early pool constituted 3 panicles (x) of 0.2 cm, 4x 0.3 cm, 4x 0.4 cm, 4x 0.5 cm. The
793 middle pool constituted 1x 0.5 cm, 2x 0.6 cm, 2x 0.7 cm, 1x 0.8 cm, 1x 0.9 cm, 1x 1 cm. The
794 late pool constituted 1x 1cm, 1x 1.2 cm, 1x 1.5 cm, 1x 2cm. For each pool, the number of
795 biological replicates of WT and *osmads2*$^{d8/d8}$ tissues was three and two, respectively. First, total
796 RNA was extracted from panicle tissue using the TRIzol R reagent (Invitrogen, Carlsbad, CA,
797 USA). RNA was then treated with DNAse I (M0303S NEB, Massachusetts, USA) to remove

contaminating gDNA according to the manufacturer's protocol. RNA quality and concentration were examined on a 4150 TapeStation (Catalog: G2992AA, Agilent Technologies, California, USA) and Qubit (Life Technologies, California, USA), respectively. RNA of integrity number (RIN) > 7 was used for library construction. Total RNA of 500 ng was used to enrich mRNA using the NEBNext Poly (A) mRNA magnetic isolation module (Catalog: E7490, New England Biolabs) following the manufacturer's protocol. Enriched mRNAs were used for library preparation using the NEBNext® Ultra™ II RNA Library Prep Kit for Illumina (Catalog: E7775S, New England Biolabs). Sequence data was generated using the Illumina HiSeq, pair-end 2X150bp chemistry. Sequencing depth ranged from 14 million to 31 million paired-end reads per sample. Data was checked for base call quality distribution, percentage of bases above Q20, Q30, %GC, and sequencing adapter contamination using FastQC and MultiQC software (Ewels et al., 2016). All the samples passed the QC threshold (Q30>90%). Raw sequence reads were processed to remove adapter sequences and low-quality bases using fastp (Chen et al., 2018). The QC passed reads were then mapped onto the indexed *Oryza sativa* ssp. japonica cv. reference genome (RAP-DB; https://rapdb.dna.affrc.go.jp/), using the STAR v2 aligner (Dobin et al., 2013). On average, 99.9% of the reads aligned to the reference genome. Raw reads were counted with the featureCounts function from the Rsubread package (Liao et al., 2019). Differential expression analysis was carried out using the edgeR package (Robinson et al., 2010) after normalizing the read counts based on trimmed mean of M (TMM) values. Replicates from *osmads2*$^{d8d/d8}$ were compared to replicates from WT. Genes with an absolute log2 fold change ≥ 1 and an adjusted p-value ≤ 0.05 were considered significant. The RNA-Seq raw data from 6-week-old SAMs of rice (Gómez-Ariza et al., 2019) were downloaded from NCBI and mapped as described above. The RNA-Seq raw data from 9-day old SAMs of *Arabidopsis* (Klepikova et al., 2015) were downloaded from NCBI and mapped to the TAIR9 Genome Release. Hypergeometric GO enrichment analysis was conducted by using GO annotations of Oryzabase (https://shigen.nig.ac.jp/rice/oryzabase/locale/change?lang=en) as the global dataset, and *osmads2* DEG datasets as local datasets. Significantly enriched GO terms (qValue ≤ 0.05) and the associated genes were curated in a supplemental dataset. For orthologous group analysis, a list of orthologous groups (file name: APK_ftp_file.txt) was downloaded from the Rice Genome Annotation Project (http://rice.uga.edu/annotation_pseudo_apk.shtml). This list was reorganized to contain only rice genes with corresponding *Arabidopsis* orthologs, and then downsized to only those rice genes that were differentially expressed in at least one stage. This list was then overlapped with the *pi-1* dataset (Wuest et al., 2012) to identify the rice

832 downstream targets of OsMADS2 that have an ortholog represented in *pi-1* data set of
833 differentially expressed genes.

834 **RT-qPCR, ChIP-qPCR and RNA *in situ* hybridization**

835 Synthesizing of cDNAs, RT-qPCR reactions and calculation of fold-change were performed as
836 described in Prakash et al. (2022). Primers used and their sequences are given in Supplementary
837 Table S4. For ChIP-qPCR, WT TP309 panicles of length 0.5-1 cm or 1-2 cm (~200mg) were
838 used. The tissues were fixed with 1% formaldehyde in fixation buffer. OsMADS2 ChIP was
839 performed using the SimpleChIP® Enzymatic Chromatin IP Kit (Cat #9002, CST,
840 Massachusetts, USA). MNaseI-based chromatin was prepared with a DNA size range of 150bp
841 to 900bp. For the ChIP, 2 µl were kept as input DNA and 90 µl of chromatin was taken and
842 incubated with 6µg of affinity-purified anti-OsMADS2 antibody overnight. The DNA-protein
843 complexes were pulled down using protein-A magnetic beads. Simultaneously, a negative
844 control sample (Mock IP, no primary antibody) was processed similarly. Immunoprecipitated
845 DNA was eluted using the elution buffer provided in the kit and reverse cross-linked using 2M
846 RNase A, 4M proteinase K in 5M NaCl for 6 hours at 65˚C. The DNA was then purified using
847 column purification. For ChIP-qPCR, the final ChIP DNA was diluted 10 times and 1 µl was
848 used for qPCR with locus-specific primers (Appendix D). For each tested locus, two regions
849 (peak and nonpeak) were amplified using DNA from input, IPed, and mock samples. First
850 %input was calculated as follows: %input for IP samples= 2^(CT.in-log2(DF)-CT.ip) and
851 %input for Mock samples= 2^(CT.in-log2(DF)-CT.mock). CT.in, CT.ip, and CT.mock refer to
852 the average CT value for input, IPed, and mock samples respectively. DF refers to the dilution
853 factor of the input. The relative enrichment was then calculated by dividing the %input in the
854 peak region to %input in the nonpeak region. Hence, the values for the nonpeak regions were
855 all set to 1. The data were derived from two independent biological replicates of OsMADS2
856 ChIPed DNA along with respective Mock sample, each include two technical replicates. The
857 *in situ* hybridization experiments were performed as described by Yadav et al. (2007), using
858 *OsMADS2* gene-specific RNA probe of ~644bp cDNA sequences, excluding the MADS
859 domain (Nandi et al., 2000), *OsMADS4* gene-specific RNA probe of 289bp cDNA sequences
860 contain the C terminal and 3'UTR (Yadav et al., 2007) and gene-specific RNA probes for
861 *CYCLIN-P4-1-LIKE*, *PIP1-1* and *PTR2* (Supplementary Table 3).

862 **Inference of Gene Regulatory Networks**

863 We overlapped 2,589 OsMADS2-bound genes (ChIP-Seq output) with the DEGs (1.5-fold
864 change and FDR ≤ 0.05, RNA-Seq output) from two progressive inflorescence stages (early

865 and middle pools) to identify direct target genes (genes common to ChIP-Seq and RNA-Seq
866 datasets). Transcription factors from these direct targets were extracted and used as first layer
867 nodal genes to link OsMADS2 regulation to its indirectly regulated downstream genes (DEGs
868 that are not present in the ChIP-Seq dataset). For this, promotor analysis was conducted to
869 identify indirect targets with at least a single occurrence of DNA-binding motifs for WRKY8
870 (TTGACY), ERF65 (AGCCGCC), OsHOX2 (CAAT(G/C)ATTG), OsHOX4
871 (CAAT(T/A)ATTG), OsARF7A (TGTCTC), OsPCF2 (GGNCCCAC), OsPCF5
872 (GTGGNCCC), OsSPL2 (TNCGTACAA), and HSFC1B (TTCTAGAA/GAANNTTC).
873 Occurrences of these motifs were checked in 600 bp of assumed promotor sequence (-500 to
874 +100 bp with respect to the TSS). The binding site information was retrieved from the
875 PlantPAN3.0 database (Chow et.al., 2019). Cytoscape software (Shannon et al., 2003) was used
876 to draw the network.

877 **Statistical Analysis**

878 Student's *t* tests and Chi-square were performed using the GraphPad Prism software (version
879 9.0.0). Chi-square was used to test conformity of observed segregation ratio with expected
880 Mendelian ratio. Two-tailed Student's *t* tests used to compare the differences between two
881 groups. Multiple unpaired Student's *t* tests were used to compares the means of multiple groups.
882 The number of individuals and replicates is indicated for each experiment either in the figure
883 legends or the materials and methods section. P values <0.05 were considered statistically
884 significant. The results of the statistical analyses are listed in Supplementary Data Set S6.

885 **Accession numbers**

886 RNA-Seq and ChIP-Seq data obtained in this study are deposited to NCBI Gene Expression
887 Omnibus (https://www.ncbi.nlm.nih.gov/geo/query/acc.cgi) with number GSE260916 and
888 GSE260918 and will become publicly available immediately upon publication. Other public
889 transcriptome data obtained from NCBI Sequence Read Archive (https://www.ncbi.nlm.
890 nih.gov/sra) are for 6-week-old SAMs of rice: SRR5052708 and 9-day-old SAMs of
891 *Arabidopsis*: SRR2073174. The accession numbers, as per RAP database
892 (https://rapdb.dna.affrc.go.jp/), for genes mentioned in results section are as follow:
893 *OsMADS2*: Os01g0883100; *OsMADS4*: Os05g0423400; *GH9B16*: Os08g0114200; *HSFC1B*:
894 Os01g0733200; *PCF2*: Os08g0544800; *PTR2*: Os12g0638200; *CYCLIN-P4-1-LIKE*:
895 Os07g0231500; *EGL1*: Os05g0375400; *YUC1*: Os01g0645400; *YUC3*: Os01g0732700;
896 *YUC7*: Os04g0128900; *TDD1*: Os04g0463500; *NIT1*: Os02g0635200; *GI*: Os01g0182600;
897 *OsMADS50*: Os03g0122600; Os*MADS55*: Os06g0217300; *HOX1*: Os10g0561800; *IIP3*:

898 Os02g0575700; *PME24*: Os08g0220400; *BGLU30*: Os09g0491100; *TPKb*: Os07g0108800;
899 *TIP4-1*: Os05g0231700; *TIP4-3*: Os01g0232000; *PIP1A*: Os02g0666200; *SPL16*:
900 Os08g0531600; *FON1*: Os06g0717200; *TDR*: Os01g0293100; *MTR1*: Os02g0491300; *SPL*:
901 Os05g0501800; *ESP*: Os01g0356951; *GA20ox4*: Os05g0421900; *MADS13*: Os12g0207000;
902 *DFOT1*: Os01g0611000; *HOX12*: Os03g0198600; *JAZ6*: Os03g0402800; *JAZ7*:
903 Os07g0615200; *KRP3*: Os11g0614800.

904 **Supplementary Data**

905 **Supplementary Figure S1**. Generation and characterization of CRISPR/Cas9-derived
906 *osmads2* heritable mutant alleles.

907 **Supplementary Figure S2**. Additional phenotypic analysis of the different genotypes studied.

908 **Supplementary Figure S3.** Supporting histological analysis of floral organs in different
909 genotypes studied.

910 **Supplementary Figure S4.** Analysis of pollen viability in the different genotypes studied.

911 **Supplementary Figure S5.** Expression analysis (fold-change) of the B-class genes *OsMADS2*
912 and *OsMADS4* in *osmads4kd#1* transgenics.

913 **Supplementary Figure S6.** Analysis of flowering time in different genotypes studied and
914 meta-analysis of expression status of B-class MADS domain genes in rice and *Arabidopsis*
915 shoot apical meristems.

916 **Supplementary Figure S7.** Characterization of the integration site and illustration of
917 genotyping for zygosity of the *OsMADS4* dsRNAi cassette.

918 **Supplementary Figure S8.** Scanning electron micrographs (SEM) of developing floral
919 meristems and floret primordia in WT and rice *PI*-clade gene variants *osmads2*$^{d8/d8}$ and
920 *osmads2*$^{d8/d8}$ *osmads4kd*.

921 **Supplementary Figure S9.** Supporting histological analyses of ovule differentiation in WT
922 and *osmads2 osmads4kd* doubly perturbed florets.

923 **Supplementary Figure S10.** Supporting analyses for DNA *cis*-regulatory motifs in peak
924 regions bound by OsMADS2 and ChIP-qPCR validation of binding at *EGL1*.

925 **Supplementary Figure 11**. Supporting gene expression analyses.

926 **Supplementary Figure S12.** Gene Regulatory Network constructed based on ChIP-Seq and
927 transcriptome data (RNA-Seq, tissue pool constituting 0.2-0.5 cm panicles).

928 **Supplementary Figure S13.** An OsMADS2 Gene Regulatory Network (GRN) constructed
929 based on ChIP-Seq and transcriptome data (RNA-Seq, tissue pool constituting 0.5-1 cm
930 panicles).

931 **Supplementary Figure S14.** Supporting spatiotemporal gene expression analysis of
932 OsMADS2 targets and characterization of the WT lodicule.
933 **Supplementary Table S1:** Analysis of segregation of different *osmads2* mutant alleles using
934 the Chi-square test.
935 **Supplementary Table S2:** Summary of spikelet phenotyping data for WT and *osmads*$^{d8/d8}$
936 **Supplementary Table S3:** Summary of genotyping and phenotyping data from the two
937 phenotypic groups of *osmads2 osmads4kd* double mutant plants.
938 **Supplementary Table S4:** Sequences of the different primers and oligos used in this study
939 **Supplementary Data Set 1:** ChIP-Seq peaks enriched in an anti-OsMADS2 ChIP experiment.
940 **Supplementary Data Set 2:** List of DEGs in different *osmads2* data sets.
941 **Supplementary Data Set 3:** List of Gene Ontology (GO) terms enriched in different *osmads2*
942 DEG subsets
943 **Supplementary Data Set 4:** List of DEGs in *osmads2* that have orthologs deregulated in the
944 *Arabidopsis pi-1* mutant
945 **Supplementary Data Set 5:** Supporting analysis of the GRNs. List of DEGs in early and middle
946 *osmads2* expression data sets with respective number of DNA binding motifs for the different
947 nodal transcription factors.
948 **Supplementary Data Set 6:** Supplementary Data Set 6. Summary of statistical analyses

949 **Acknowledgments**
950 We acknowledge the DBT-IISc Partnership Divisional Bio-imaging and Greenhouse Facilities.
951 We thank the Functional Genomics Center Zurich for access to its excellent infrastructure to
952 perform next-generation sequencing for the ChIP-Seq experiment. We thank Prof. MS
953 Sheshshayee, University of Agricultural Sciences, GKVK, Bangalore, for providing access to
954 instrument and technical assist for measuring the osmolality. We thank Saurabh Bhatt from
955 UVR laboratory for generating the PTR2 specific clone used for RNA *in situ* hybridization.
956 We acknowledge inputs from members of the UVR laboratory during the course of this study
957 and inputs from Prof. Kalika Prasad, IISER Pune, during the course of manuscript preparation.
958 We also thank Murthy and Jagadeesh for assistance in plant growth and care in field plots and
959 transgenic greenhouses.

960 **Funding**
961 This study was funded by the Department of Biotechnology, Ministry of Science and
962 Technology, Government of India, grant No. BT/PR38988/AGIII/103/1232/2020 to U.V. This
963 work was also supported by the University of Zurich, a grant of the Swiss National Science

964 Foundation (31003A_179553 to U.G.), and an Infosys Visiting Chair Professorship (to U.G.).
965 Research fellowships to M.Z., S.P. and R.P. were received from the Indian Institute of Science.
966 RB is supported by the Prime Minister's Research Fellowship, Ministry of Education,
967 Government of India. M.Z. is currently funded by the International Visiting Faculty Program
968 of the Indian Institute of Science. U.V. holds the J N Tata Chair at the Indian Institute of
969 Science.

970 **Author contributions**

971 UV, UG and MZ designed the research. MZ, SS[1], SP, RB, IK, and SS[2] performed the
972 experiments. RP and MZ performed the bioinformatic analyses. Manuscript writing was done
973 by MZ, UG, and UV with contributions from IK and SS. All authors read and approved the
974 final manuscript.

975 **References**

976 **Abu-Zaitoon YM.** Phylogenetic analysis of putative genes involved in the tryptophan-
977 dependent pathway of auxin biosynthesis in rice. Appl Biochem Biotechnol.
978 2014:**172**(5):2480–2495. https://doi.org/10.1007/S12010-013-0710-4/FIGURES/7

979 **Ahmad I, Devonshire J, Mohamed R, Schultze M, and Maathuis FJM**. Overexpression of
980 the potassium channel TPKb in small vacuoles confers osmotic and drought tolerance to rice.
981 New Phytol. 2016:**209**(3):1040–1048. https://doi.org/10.1111/NPH.13708

982 **Akiyama T, Jin S, Yoshida M, Hoshino T, Opassiri R, and Ketudat Cairns JR**. Expression
983 of an endo-(1,3;1,4)-beta-glucanase in response to wounding, methyl jasmonate, abscisic acid
984 and ethephon in rice seedlings. J Plant Physiol. 2009:**166**(16):1814–1825.
985 https://doi.org/10.1016/J.JPLPH.2009.06.002

986 **Ambrose BA, Lerner DR, Ciceri P, Padilla CM, Yanofsky MF, and Schmidt RJ**.
987 Molecular and Genetic Analyses of the *Silky1* Gene Reveal Conservation in Floral Organ
988 Specification between Eudicots and Monocots. Mol Cell. 2000:**5**(3):569–579.
989 https://doi.org/10.1016/S1097-2765(00)80450-5

990 **Balázsi G, Van Oudenaarden A, and Collins JJ**. Cellular decision making and biological
991 noise: from microbes to mammals. Cell. 2011:**144**(6):910–925.
992 https://doi.org/10.1016/J.CELL.2011.01.030

993 **Bartlett ME, Williams SK, Taylor Z, Deblasio S, Goldshmidt A, Hall DH, Schmidt RJ,**
994 **Jackson DP, and Whipplea CJ**. The Maize *PI/GLO* Ortholog *Zmm16/sterile tassel silky ear1*
995 Interacts with the Zygomorphy and Sex Determination Pathways in Flower Development. Plant
996 Cell. 2015:**27**(11):3081–3098. https://doi.org/10.1105/TPC.15.00679

997 **Bowman JL, Smyth DR, and Meyerowitz EM**. Genes directing flower development in
998 *Arabidopsis*. Plant Cell. 1989:**1**(1):37–52. https://doi.org/10.1105/TPC.1.1.37
999 **Busk PK and Pagès M**. Microextraction of Nuclear Proteins from Single Maize Embryos.
1000 Plant Mol Biol Report. 1997:**15**(4):371–376.
1001 https://doi.org/10.1023/A:1007428802474/METRICS
1002 **Cao L, Tian J, Liu Y, Chen X, Li S, Persson S, Lu D, Chen M, Luo Z, Zhang D, et al.**
1003 Ectopic expression of OsJAZ6, which interacts with OsJAZ1, alters JA signaling and spikelet
1004 development in rice. Plant J. 2021:**108**(4):1083–1096. https://doi.org/10.1111/TPJ.15496
1005 **Chen S, Zhou Y, Chen Y, and Gu J**. fastp: an ultra-fast all-in-one FASTQ preprocessor.
1006 Bioinformatics. 2018:**34**(17):i884–i890.
1007 https://doi.org/10.1093/BIOINFORMATICS/BTY560
1008 **Choi MG, Kim EJ, Song JY, Choi SB, Cho SW, Park CS, Kang CS, and Park Y Il**. Peptide
1009 transporter2 (PTR2) enhances water uptake during early seed germination in *Arabidopsis*
1010 *thaliana*. Plant Mol Biol. 2020:**102**(6):615–624. https://doi.org/10.1007/s11103-020-00967-3
1011 **Chow CN, Lee TY, Hung YC, Li GZ, Tseng KC, Liu YH, Kuo PL, Zheng HQ, and Chang**
1012 **WC**. PlantPAN3.0: a new and updated resource for reconstructing transcriptional regulatory
1013 networks from ChIP-seq experiments in plants. Nucleic Acids Res. 2019:**47**(D1):D1155–
1014 D1163. https://doi.org/10.1093/NAR/GKY1081
1015 **Chung YY, Kim SR, Kang HG, Noh YS, Park MC, Finkel D, and An G**. Characterization
1016 of two rice MADS box genes homologous to *GLOBOSA*. Plant Sci. 1995:**109**(1):45–56.
1017 https://doi.org/10.1016/0168-9452(95)04153-L
1018 **Coen ES and Meyerowitz EM**. The war of the whorls: genetic interactions controlling flower
1019 development. Nat 1991 3536339. 1991:**353**(6339):31–37. https://doi.org/10.1038/353031a0
1020 **Cosgrove DJ**. Enzymes and other agents that enhance cell wall extensibility. Annu Rev Plant
1021 Physiol Plant Mol Biol. 1999:**50**:391–417.
1022 https://doi.org/10.1146/ANNUREV.ARPLANT.50.1.391
1023 **Dobin A, Davis CA, Schlesinger F, Drenkow J, Zaleski C, Jha S, Batut P, Chaisson M,**
1024 **and Gingeras TR**. STAR: ultrafast universal RNA-seq aligner. Bioinformatics.
1025 2013:**29**(1):15–21. https://doi.org/10.1093/BIOINFORMATICS/BTS635
1026 **Doi K, Izawa T, Fuse T, Yamanouchi U, Kubo T, Shimatani Z, Yano M, and Yoshimura**
1027 **A**. Ehd1, a B-type response regulator in rice, confers short-day promotion of flowering and
1028 controls *FT*-like gene expression independently of Hd1. Genes Dev. 2004:**18**(8):926.
1029 https://doi.org/10.1101/GAD.1189604

1030 **Dreni L, Jacchia S, Fornara F, Fornari M, Ouwerkerk PBF, An G, Colombo L, and Kater**
1031 **MM**. The D-lineage MADS-box gene *OsMADS13* controls ovule identity in rice. Plant J.
1032 2007:**52**(4):690–699. https://doi.org/10.1111/J.1365-313X.2007.03272.X
1033 **Elowitz MB, Levine AJ, Siggia ED, and Swain PS**. Stochastic gene expression in a single
1034 cell. Science. 2002:**297**(5584):1183–1186. https://doi.org/10.1126/SCIENCE.1070919
1035 **Ewels P, Magnusson M, Lundin S, and Käller M**. MultiQC: summarize analysis results for
1036 multiple tools and samples in a single report. Bioinformatics. 2016:**32**(19):3047–3048.
1037 https://doi.org/10.1093/BIOINFORMATICS/BTW354
1038 **Favaro R, Pinyopich A, Battaglia R, Kooiker M, Borghi L, Ditta G, Yanofsky MF, Kater**
1039 **MM, and Colombo L**. MADS-Box Protein Complexes Control Carpel and Ovule
1040 Development in *Arabidopsis*. Plant Cell. 2003:**15**(11):2603–2611.
1041 https://doi.org/10.1105/TPC.015123
1042 **Gao S, Fang J, Xu F, Wang W, and Chu C**. Rice HOX12 regulates panicle exsertion by
1043 directly modulating the expression of ELONGATED UPPERMOST INTERNODE1. Plant
1044 Cell. 2016:**28**(3):680–695. https://doi.org/10.1105/TPC.15.01021
1045 **Gómez-Ariza J, Brambilla V, Vicentini G, Landini M, Cerise M, Carrera E, Shrestha R,**
1046 **Chiozzotto R, Galbiati F, Caporali E, et al.** A transcription factor coordinating internode
1047 elongation and photoperiodic signals in rice. Nat Plants 2019 54. 2019:**5**(4):358–362.
1048 https://doi.org/10.1038/s41477-019-0401-4
1049 **Gonçalves B, Nougué O, Jabbour F, Ridel C, Morin H, Laufs P, Manicacci D, and**
1050 **Damerval C**. An APETALA3 homolog controls both petal identity and floral meristem
1051 patterning in *Nigella damascena* L. (Ranunculaceae). Plant J. 2013:**76**(2):223–235.
1052 https://doi.org/10.1111/TPJ.12284
1053 **Hayama R, Yokoi S, Tamaki S, Yano M, and Shimamoto K**. Adaptation of photoperiodic
1054 control pathways produces short-day flowering in rice. Nat 2003 4226933.
1055 2003:**422**(6933):719–722. https://doi.org/10.1038/nature01549
1056 **Heslop-Harrison Y and Heslop-Harrison JS**. Lodicule function and filament extension in
1057 the grasses: Potassium ion movement and tissue specialization. Ann Bot. 1996:**77**(6):573–582.
1058 https://doi.org/10.1093/AOB/77.6.573
1059 **Hill TA, Day CD, Zondlo SC, Thackeray AG, and Irish VF**. Discrete spatial and temporal
1060 cis-acting elements regulate transcription of the *Arabidopsis* floral homeotic gene *APETALA3*.
1061 Development. 1998:**125**(9):1711–1721. https://doi.org/10.1242/DEV.125.9.1711
1062 **Hu Y, Wang L, Jia R, Liang W, Zhang X, Xu J, Chen X, Lu D, Chen M, Luo Z, et al.** Rice
1063 transcription factor MADS32 regulates floral patterning through interactions with multiple

1064 floral homeotic genes. J Exp Bot. 2021:**72**(7):2434–2449.
1065 https://doi.org/10.1093/JXB/ERAA588
1066 **Jack T, Fox GL, and Meyerowitz EM**. *Arabidopsis* homeotic gene *APETALA3* ectopic
1067 expression: transcriptional and posttranscriptional regulation determine floral organ identity.
1068 Cell. 1994:**76**(4):703–716. https://doi.org/10.1016/0092-8674(94)90509-6
1069 **Ji J and Braam J**. Restriction Site Extension PCR: A novel method for high-throughput
1070 characterization of tagged DNA fragments and genome walking. PLoS One. 2010:**5**(5):e10577.
1071 https://doi.org/10.1371/JOURNAL.PONE.0010577
1072 **Joldersma D and Liu Z**. The making of virgin fruit: the molecular and genetic basis of
1073 parthenocarpy. J Exp Bot. 2018:**69**(5):955–962. https://doi.org/10.1093/JXB/ERX446
1074 **Kang HG, Jeon JS, Lee S, and An G**. Identification of class B and class C floral organ identity
1075 genes from rice plants. Plant Mol Biol. 1998:**38**(6):1021–1029.
1076 https://doi.org/10.1023/A:1006051911291/METRICS
1077 **Kaufmann K, Muiño JM, Jauregui R, Airoldi CA, Smaczniak C, Krajewski P, and**
1078 **Angenent GC**. Target genes of the MADS transcription factor SEPALLATA3: integration of
1079 developmental and hormonal pathways in the *Arabidopsis* flower. PLoS Biol. 2009:**7**(4):0854–
1080 0875. https://doi.org/10.1371/JOURNAL.PBIO.1000090
1081 **Klepikova A V., Logacheva MD, Dmitriev SE, and Penin AA**. RNA-seq analysis of an
1082 apical meristem time series reveals a critical point in *Arabidopsis thaliana* flower initiation.
1083 BMC Genomics. 2015:**16**(1):1–16. https://doi:10.1186/s12864-015-1688-9
1084 **Krizek BA and Fletcher JC**. Molecular mechanisms of flower development: an armchair
1085 guide. Nat Rev Genet 2005 69. 2005:**6**(9):688–698. https://doi.org/10.1038/nrg1675
1086 **Krizek BA and Meyerowitz EM**. The *Arabidopsis* homeotic genes *APETALA3* and
1087 *PISTILLATA* are sufficient to provide the B class organ identity function. Development.
1088 1996:**122**(1):11–22. https://doi.org/10.1242/DEV.122.1.11
1089 **Krizek BA**. Auxin regulation of Arabidopsis flower development involves members of the
1090 AINTEGUMENTA-LIKE/PLETHORA (AIL/PLT) family. J Exp Bot. 2011:**62**(10):3311–
1091 3319. https://doi.org/10.1093/JXB/ERR127
1092 **Lee JH, Park SH, and Ahn JH**. Functional conservation and diversification between rice
1093 OsMADS22/OsMADS55 and *Arabidopsis* SVP proteins. Plant Sci. 2012:**185**–**186**:97–104.
1094 https://doi.org/10.1016/J.PLANTSCI.2011.09.003
1095 **Lee S, Jeon JS, An K, Moon YH, Lee S, Chung YY, and An G**. Alteration of floral organ
1096 identity in rice through ectopic expression of *OsMADS16*. Planta. 2003:**217**(6):904–911.
1097 https://doi.org/10.1007/S00425-003-1066-8

1098 **Li N, Zhang DS, Liu HS, Yin CS, Li XX, Liang WQ, Yuan Z, Xu B, Chu HW, Wang J, et**
1099 **al.** The rice *tapetum degeneration retardation* gene is required for tapetum degradation and
1100 anther development. Plant Cell. 2006:**18**(11):2999–3014.
1101 https://doi.org/10.1105/TPC.106.044107
1102 **Li Q, Tong T, Jiang W, Cheng J, Deng F, Wu X, Chen ZH, Ouyang Y, and Zeng F**. Highly
1103 Conserved Evolution of Aquaporin PIPs and TIPs Confers Their Crucial Contribution to
1104 Flowering Process in Plants. Front Plant Sci. 2022:**12**:2945.
1105 https://doi.org/10.3389/FPLS.2021.761713/BIBTEX
1106 **Li S, Wei K, Zhang L, Ning Y, Lu F, Wang X, Guo Y, Liu L, Li X, Zhu C, et al.** Fine
1107 mapping and candidate gene validation of tomato gene *Carpelloid Stamen and Parthenocarpy*
1108 (*CSP*). Horticulturae. 2024:**10**(4):403.
1109 https://doi.org/10.3390/HORTICULTURAE10040403/S1
1110 **Li Y, Ouyang J, Wang YY, Hu R, Xia K, Duan J, Wang Y, Tsay YF, and Zhang M**.
1111 Disruption of the rice nitrate transporter OsNPF2.2 hinders root-to-shoot nitrate transport and
1112 vascular development. Sci Reports 2015 51. 2015:**5**(1):1–10.
1113 https://doi.org/10.1038/srep09635
1114 **Liang M, Deng L, Liu J, He A, and Chen L.** Interaction between the *eui* gene and thermo-
1115 sensitive genic male sterility in rice. Euphytica. 2008:**164**(3):637–643.
1116 https://doi.org/10.1007/S10681-008-9657-X/TABLES/2
1117 **Liao Y, Smyth GK, and Shi W**. The R package Rsubread is easier, faster, cheaper and better
1118 for alignment and quantification of RNA sequencing reads. Nucleic Acids Res.
1119 2019:**47**(8):e47–e47. https://doi.org/10.1093/NAR/GKZ114
1120 **Lohmann JU and Weigel D**. Building beauty: the genetic control of floral patterning. Dev
1121 Cell. 2002:**2**(2):135–142. https://doi.org/10.1016/S1534-5807(02)00122-3
1122 **Luan X, Liu S, Ke S, Dai H, Xie XM, Hsieh TF, and Zhang XQ**. Epigenetic modification
1123 of *ESP*, encoding a putative long noncoding RNA, affects panicle architecture in rice. Rice.
1124 2019:**12**(1). https://doi.org/10.1186/S12284-019-0282-1
1125 **Machanick P and Bailey TL**. MEME-ChIP: motif analysis of large DNA datasets.
1126 Bioinformatics. 2011:**27**(12):1696–1697.
1127 https://doi.org/10.1093/BIOINFORMATICS/BTR189
1128 **Mizutani M, Naganuma T, Tsutsumi KI, and Saitoh Y**. The syncytium-specific expression
1129 of the Orysa;KRP3 CDK inhibitor: implication of its involvement in the cell cycle control in
1130 the rice (*Oryza sativa* L.) syncytial endosperm. J Exp Bot. 2010:**61**(3):791–798.
1131 https://doi.org/10.1093/JXB/ERP343

1132 **Nagasawa N, Miyoshi M, Sano Y, Satoh H, Hirano H, Sakai H, and Nagato Y**.
1133 *SUPERWOMAN1* and *DROOPING LEAF* genes control floral organ identity in rice.
1134 Development. 2003:**130**(4):705–718. https://doi.org/10.1242/DEV.00294
1135 **Nandi Ak, Kushalappa K, Prasad K, and Vijayraghavan U**. A conserved function for
1136 *Arabidopsis SUPERMAN* in regulating floral-whorl cell proliferation in rice, a
1137 monocotyledonous plant. Curr Biol. 2000:**10**(4):215–218. https://doi.org/10.1016/S0960-
1138 9822(00)00341-9
1139 **Ning J, Zhang B, Wang N, Zhou Y, and Xiong L**. Increased Leaf Angle1, a Raf-Like
1140 MAPKKK that interacts with a nuclear protein family, regulates mechanical tissue formation
1141 in the lamina joint of rice. Plant Cell. 2011:**23**(12):4334–4347.
1142 https://doi.org/10.1105/TPC.111.093419
1143 **O'Toole JC and Namuco OS**. Role of panicle exsertion in water stress induced sterility. Crop
1144 Sci. 1983:**23**(6):1093–1097.
1145 https://doi.org/10.2135/CROPSCI1983.0011183X002300060017X
1146 **Pagès H, Aboyoun P, Gentleman R, and DebRoy S.** *Biostrings: Efficient manipulation of*
1147 *biological strings*. R package version 2.64.0,
1148 (2022). https://bioconductor.org/packages/Biostrings
1149 **Pinyopich A, Ditta GS, Savidge B, Liljegren SJ, Baumann E, Wisman E, and Yanofsky**
1150 **MF**. Assessing the redundancy of MADS-box genes during carpel and ovule development. Nat
1151 2003 4246944. 2003:**424**(6944):85–88. https://doi.org/10.1038/nature01741
1152 **Prakash S, Rai R, Zamzam M, Ahmad O, Peesapati R, and Vijayraghavan U**. OsbZIP47
1153 is an integrator for meristem regulators during rice plant growth and development. Front Plant
1154 Sci. 2022:**13**:883. https://doi.org/10.3389/FPLS.2022.865928/BIBTEX
1155 **Prasad K and Vijayraghavan U**. Double-stranded RNA interference of a rice *PI/GLO*
1156 paralog, *OsMADS2*, uncovers its second-whorl-specific function in floral organ patterning.
1157 Genetics. 2003:**165**(4):2301–2305. https://doi.org/10.1093/GENETICS/165.4.2301
1158 **Ren L, Tang D, Zhao T, Zhang F, Liu C, Xue Z, Shi W, Du G, Shen Y, Li Y, et al.** OsSPL
1159 regulates meiotic fate acquisition in rice. New Phytol. 2018:**218**(2):789–803.
1160 https://doi.org/10.1111/NPH.15017
1161 **Robinson MD, McCarthy DJ, and Smyth GK**. edgeR: a Bioconductor package for
1162 differential expression analysis of digital gene expression data. Bioinformatics.
1163 2010:**26**(1):139–140. https://doi.org/10.1093/BIOINFORMATICS/BTP616
1164 **Ryu CH, Lee S, Cho LH, Kim SL, Lee YS, Choi SC, Jeong HJ, Yi J, Park SJ, Han CD, et**
1165 **al.** OsMADS50 and OsMADS56 function antagonistically in regulating long day (LD)-

1166 dependent flowering in rice. Plant Cell Environ. 2009:**32**(10):1412–1427.
1167 https://doi.org/10.1111/J.1365-3040.2009.02008.X
1168 **Scarpella E, Rueb S, Boot KJM, Hoge JHC, and Meijer AH**. A role for the rice homeobox
1169 gene *Oshox1* in provascular cell fate commitment. Development. 2000:**127**(17):3655–3669.
1170 https://doi.org/10.1242/DEV.127.17.3655
1171 **Schmidt R, Schippers JHM, Welker A, Mieulet D, Guiderdoni E, and Mueller-Roeber B**.
1172 Transcription factor OsHsfC1b regulates salt tolerance and development in *Oryza sativa* ssp.
1173 japonica. AoB Plants. 2012:**2012**(1). https://doi.org/10.1093/AOBPLA/PLS011
1174 **Selva C, Yang X, Shirley NJ, Whitford R, Baumann U, and Tucker MR**. HvSL1 and
1175 HvMADS16 promote stamen identity to restrict multiple ovary formation in barley. J Exp Bot.
1176 2023:**74**(17):5039–5056. https://doi.org/10.1093/JXB/ERAD218
1177 **Shannon P, Markiel A, Ozier O, Baliga NS, Wang JT, Ramage D, Amin N, Schwikowski**
1178 **B, and Ideker T**. Cytoscape: a software environment for integrated models of biomolecular
1179 interaction networks. Genome Res. 2003:**13**(11):2498–2504.
1180 https://doi.org/10.1101/GR.1239303
1181 **Shi J, Hou F, Dong Y, Pan Y, Zhou Q, Zhang Z, Liu Y, and Liu W**. Functional validation
1182 of two B-class MADS-box genes *HmPI* and *HmAP3* from *Hemerocallis middendorffii*. Vitr
1183 Cell Dev Biol - Plant. 2024:1–12. https://doi.org/10.1007/s11627-024-10470-9
1184 **Sazuka T, Kamiya N, Nishimura T, Ohmae K, Sato Y, Imamura K, Nagato Y, Koshiba**
1185 **T, Nagamura Y, Ashikari M, et al.** A *rice tryptophan deficient dwarf mutant*, *tdd1*, contains
1186 a reduced level of indole acetic acid and develops abnormal flowers and organless embryos.
1187 Plant J. 2009:**60**(2):227–241. https://doi.org/10.1111/J.1365-313X.2009.03952.X
1188 **Suzaki T, Sato M, Ashikari M, Miyoshi M, Nagato Y, and Hirano HY**. The gene *FLORAL*
1189 *ORGAN NUMBER1* regulates floral meristem size in rice and encodes a leucine-rich repeat
1190 receptor kinase orthologous to *Arabidopsis* CLAVATA1. Development. 2004:**131**(22):5649–
1191 5657. https://doi.org/10.1242/DEV.01441
1192 **Tan H, Liang W, Hu J, and Zhang D**. *MTR1* encodes a secretory fasciclin glycoprotein
1193 required for male reproductive development in rice. Dev Cell. 2012:**22**(6):1127–1137.
1194 https://doi.org/10.1016/J.DEVCEL.2012.04.011
1195 **Veronico P, Rosso LC, Melillo MT, Fanelli E, De Luca F, Ciancio A, Colagiero M, and**
1196 **Pentimone I**. Water stress differentially modulates the expression of tomato cell wall
1197 metabolism-related genes in *Meloidogyne incognita* feeding sites. Front Plant Sci.
1198 2022:**13**:776. https://doi.org/10.3389/FPLS.2022.817185/BIBTEX

1199 **Wang H, Zhang L, Cai Q, Hu Y, Jin Z, Zhao X, Fan W, Huang Q, Luo Z, Chen M, et al.**
1200 OsMADS32 interacts with PI-like proteins and regulates rice flower development. J Integr
1201 Plant Biol. 2015:**57**(5):504–513. https://doi.org/10.1111/JIPB.12248
1202 **Wang L, Li Q-L, Hu J-P, Yuan Z, Wang L, Li Q-L, Hu J-P, and Yuan Z**.
1203 Neofunctionalization of B-class genes in regulating rice flower development. Seed Biol 2024
1204 1e013. 2024a:**3**(1). https://doi.org/10.48130/SEEDBIO-0024-0012
1205 **Wang M, Zhu X, Huang Z, Chen M, Xu P, Liao S, Zhao Y, Gao Y, He J, Luo Y, et al.**
1206 Controlling diurnal flower-opening time by manipulating the jasmonate pathway accelerates
1207 development of indica–japonica hybrid rice breeding. Plant Biotechnol J. 2024b:**22**(8):2267–
1208 2281. https://doi.org/10.1111/PBI.14343
1209 **Wang M, Zhu X, Peng G, Liu M, Zhang S, Chen M, Liao S, Wei X, Xu P, Tan X, et al.**
1210 Methylesterification of cell-wall pectin controls the diurnal flower-opening times in rice. Mol
1211 Plant. 2022:**15**(6):956–972. https://doi.org/10.1016/J.MOLP.2022.04.004
1212 **Wang S, Wu K, Yuan Q, Liu X, Liu Z, Lin X, Zeng R, Zhu H, Dong G, Qian Q, et al.**
1213 Control of grain size, shape and quality by OsSPL16 in rice. Nat Genet 2012 448.
1214 2012:**44**(8):950–954. https://doi.org/10.1038/ng.2327
1215 **Winter CM, Austin RS, Blanvillain-Baufumé S, Reback MA, Monniaux M, Wu MF, Sang**
1216 **Y, Yamaguchi A, Yamaguchi N, Parker JE, et al.** LEAFY target genes reveal floral
1217 regulatory logic, cis motifs, and a link to biotic stimulus response. Dev Cell. 2011:**20**(4):430–
1218 443. https://doi.org/10.1016/J.DEVCEL.2011.03.019
1219 **Wuest SE, O'Maoileidigh DS, Rae L, Kwasniewska K, Raganelli A, Hanczaryk K, Lohan**
1220 **AJ, Loftus B, Graciet E, and Wellmer F**. Molecular basis for the specification of floral organs
1221 by APETALA3 and PISTILLATA. Proc Natl Acad Sci U S A. 2012:**109**(33):13452–13457.
1222 https://doi.org/10.1073/PNAS.1207075109/SUPPL_FILE/SD04.XLSX
1223 **Xie G, Yang B, Xu Z, Li F, Guo K, Zhang M, Wang L, Zou W, Wang Y, and Peng L**.
1224 Global identification of multiple OsGH9 family members and their involvement in cellulose
1225 crystallinity modification in rice. PLoS One. 2013:**8**(1):50171.
1226 https://doi.org/10.1371/JOURNAL.PONE.0050171
1227 **Xu P, Wu T, Ali A, Zhang H, Liao Y, Chen X, Tian Y, Wang W, Fu X, Li Y, et al.** EARLY
1228 MORNING FLOWERING1 (EMF1) regulates the floret opening time by mediating lodicule
1229 cell wall formation in rice. Plant Biotechnol J. 2022:**20**(8):1441–1443.
1230 https://doi.org/10.1111/PBI.13860

Yadav SR, Prasad K, and Vijayraghavan U. Divergent regulatory OsMADS2 functions control size, shape and differentiation of the highly derived rice floret second-whorl organ. Genetics. 2007:**176**(1):283–294. https://doi.org/10.1534/GENETICS.107.071746

Yang Y, Xiang H, and Jack T. *pistillata-5*, an *Arabidopsis* B class mutant with strong defects in petal but not in stamen development. Plant J. 2003:**33**(1):177–188. https://doi.org/10.1046/J.1365-313X.2003.01603.X

Yao JL, Dong YH, and Morris BAM. Parthenocarpic apple fruit production conferred by transposon insertion mutations in a MADS-box transcription factor. Proc Natl Acad Sci U S A. 2001:**98**(3):1306–1311. https://doi.org/10.1073/PNAS.98.3.1306

Yao SG, Ohmori S, Kimizu M, and Yoshida H. Unequal genetic redundancy of rice PISTILLATA orthologs, OsMADS2 and OsMADS4, in lodicule and stamen development. Plant Cell Physiol. 2008:**49**(5):853–857. https://doi.org/10.1093/PCP/PCN050
https://doi.org/10.1073/PNAS.0907896106/SUPPL_FILE/0907896106SI.PDF

Yoshida H, Itoh JI, Ohmori S, Miyoshi K, Horigome A, Uchida E, Kimizu M, Matsumura Y, Kusaba M, Satoh H, et al. *superwoman1*-cleistogamy, a hopeful allele for gene containment in GM rice. Plant Biotechnol J. 2007:**5**(6):835–846. https://doi.org/10.1111/J.1467-7652.2007.00291.X

Yu G, Wang LG, and He QY. ChIPseeker: an R/Bioconductor package for ChIP peak annotation, comparison and visualization. Bioinformatics. 2015:**31**(14):2382–2383. https://doi.org/10.1093/BIOINFORMATICS/BTV145

Yun D, Liang W, Dreni L, Yin C, Zhou Z, Kater MM, and Zhang D. *OsMADS16* genetically interacts with *OsMADS3* and *OsMADS58* in specifying. Mol Plant. 2013:**6**(3):743–756. https://doi.org/10.1093/mp/sst003

Zeng YX, Hu CY, Lu YG, Li JQ, and Liu XD. Diversity of abnormal embryo sacs in indica/japonica hybrids in rice demonstrated by confocal microscopy of ovaries. Plant Breed. 2007:**126**(6):574–580. https://doi.org/10.1111/J.1439-0523.2007.01380.X

Zhang Y, Liu T, Meyer CA, Eeckhoute J, Johnson DS, Bernstein BE, Nussbaum C, Myers RM, Brown M, Li W, et al. Model-based analysis of ChIP-Seq (MACS). Genome Biol. 2008:**9**(9):1–9. https://doi.org/10.1186/gb-2008-9-9-r137

Zhao ZX, Yin XX, Li S, Peng YT, Yan XL, Chen C, Hassan B, Zhou SX, Pu M, Zhao JH, et al. miR167d-ARFs module regulates flower opening and stigma size in rice. Rice. 2022:**15**(1):1–15. https://d oi: 10.1186/s12284-022-00587-z

Zhu LJ, Gazin C, Lawson ND, Pagès H, Lin SM, Lapointe DS, and Green MR. ChIPpeakAnno: A Bioconductor package to annotate ChIP-seq and ChIP-chip data. BMC Bioinformatics. 2010:**11**(1):1–10. https://doi.org/10.1186/1471-2105-11-237/TABLES/2

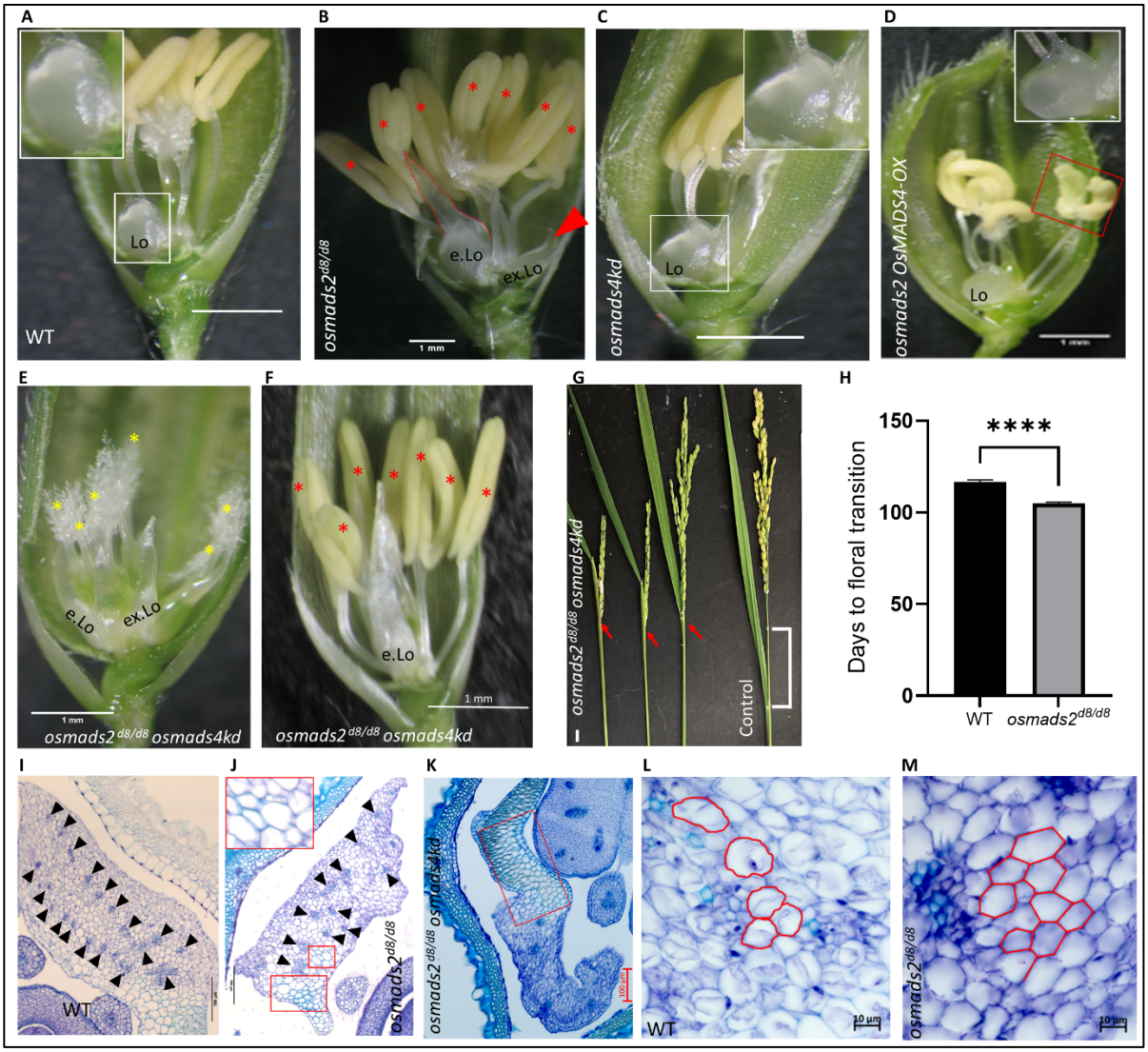

Figure 1. Phenotypic and histological analyses of the different genotypes studied. A, WT mature pre-anthesis spikelet dissected to show the lodicule. The inset shows a magnification of the normal lodicule. B, *osmads2* mutant spikelet dissected to show the abnormal organs. The red asterisks mark the increased stamen number and the red arrowhead marks the extra lodicule (ex.Lo). C, Spikelet dissected from *osmads4kd#1* showing normal floral organs. D, Spikelet from *osmads2 OsMADS4-OX* line #3 showing normal lodicule (complemented) but with abnormal crescent-like anthers (red rectangle). The number of floral organs is unchanged as compared to WT (n=300). E and F, Spikelets from *osmads2*$^{d8/d8}$ *osmads4kd* of representative group I and group II phenotypes, respectively. The yellow asterisks represent the main and ectopic carpels in group I phenotype and the red asterisks mark the increased stamen number in group II phenotype. The elongated lodicule (e.Lo) is flattened throughout the proximal distal axis (compare lodicule in E and F *vs.* in A and B). G, Panicle partial enclosure phenotype in *osmads2*$^{d8/d8}$ *osmads4kd* plants. H, Graph plot representing the number of days taken to floral transition in WT plants (n = 79) *vs.* *osmads2*$^{d8/d8}$ plants (n=125). Values are means ± the

standard error of the mean (SEM). P < 0.0001 denoted as ****; Student's *t* test. I-K, TS sections of lodicules in WT and *osmads2*$^{d8/d8}$ and *smads2*$^{d8/d8}$ *osmads4kd*, respectively. The black arrowheads mark the vascular bundles which are reduced in number and of abnormal distribution across the lodicule of *osmads2*$^{d8/d8}$. The red rectangles (in J and K) mark regions with green stained cell outlines, indicative of cell wall lignification in tissue sections stained with Toluidine blue. L and M, TS of lodicules in WT and *osmads2*$^{d8/d8}$ at high magnification showing the cell shape in the ground tissues. Compare the brick-like parenchyma in L to the polygonal like cells in M. Cell outlines are marked in red. Scale bars: 1 mm in A-F, 1 cm in G, 100 µm in I-K, 10 µm in L and M.

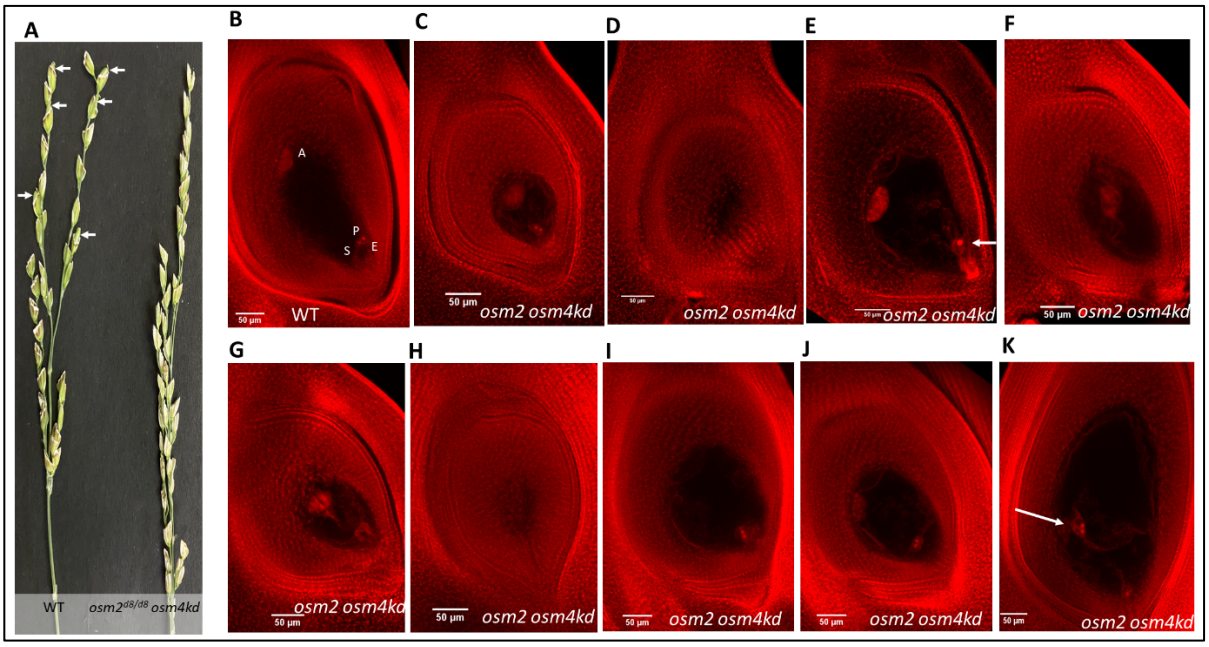

Figure 2. Female sterility in *osmads2*$^{d8/d8}$ *osmads4kd* double mutants. A, Emasculated WT and *osmads2 osmads4kd* double mutant inflorescences dusted with pollens from WT, show the development of seed (white arrows) in WT but not in *osmads2 osmads4kd* (*osm2 osm4kd*) double mutant. B-K, Ovaries and ovules from pre-anthesis WT and *osmads2 osmads4kd* florets. B, Ovule of WT with normal embryo sac constituting A; antipodal cells, P; polar nuclei, E; egg cell, S; Synergid cells. C, Ovule from *osmads2*$^{d8/d8}$ *osmads4kd* floret that has apparently normal embryo sac though smaller. D and H, Ovules with degenerated embryo sac (mass of stained cells, no full cavity). Optical sections passing through the center of the embryo sacs for panels D and H are provided in Supplementary Fig. S9, F and G, respectively. E, Embryo sac with single polar nuclei (white arrow). F, Embryo sac with no female unit (no egg cells, no polar nuclei and no synergids). G, Embryo sac with no polar nuclei. I, Embryo sac without antipodal cells. J, Embryo sac with no egg unit (no egg, no synergids). K, Embryo sac with no antipodal cells and with mislocated polar nuclei (white arrow). Scale bars in B-K are 50 µm.

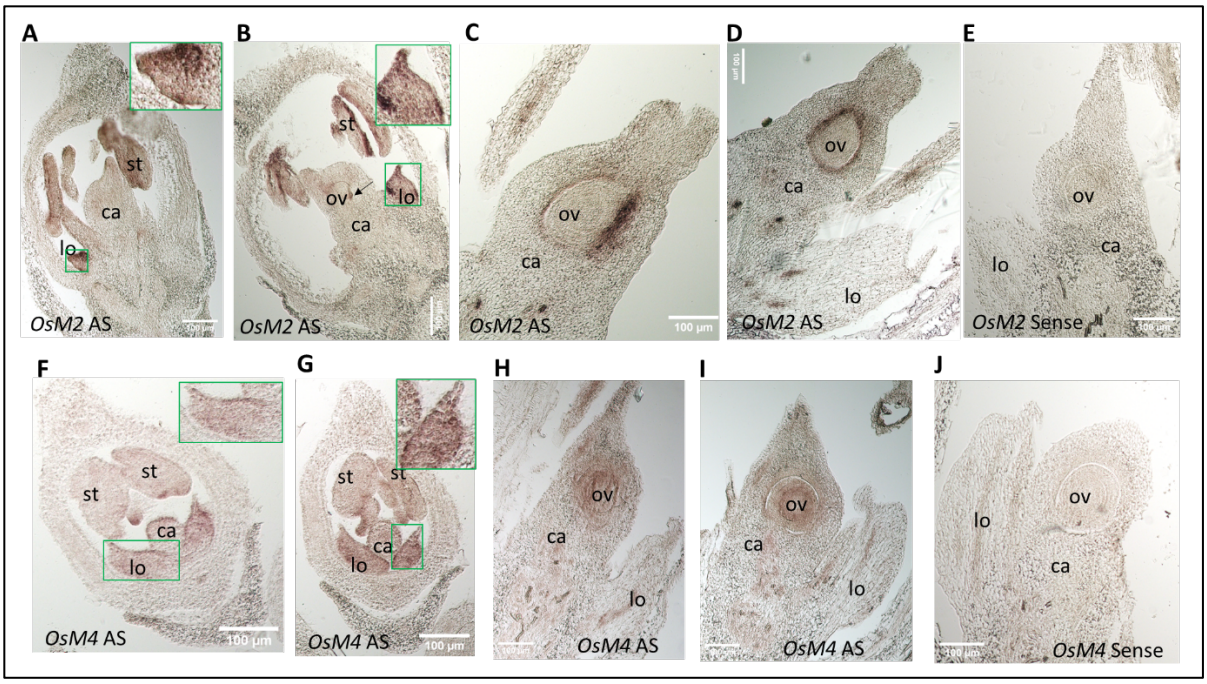

Figure 3. RNA *in situ* hybridization for *OsMADS2* and *OsMADS4* in developing ovaries with ovules. A and B, Sections showing signals for *OsMADS2* antisense probe (*OsM2* AS) in lodicules and stamens. The insets show the expression in lodicules which is enriched distally and at the edges. The black arrow in B points at signals in the initiated ovule. C and D, Sections showing *OsM2* AS signals in the inner ovary and outer layers of the developing ovules. E, Section showing no distinct signals for *OsMADS2* sense probe (*OsM2* Sense). F, Sections showing signals for *OsMADS4* antisense probe (*OsM4* AS) in lodicules and stamens. The insets show uniform expression in lodicules. H and I, Sections showing *OsM4* AS signals in the developing ovules. E, Section showing no distinct signals for *OsMADS4* sense probe (*OsM4* Sense). Abbreviations: lo; lodicule, ca, carpel, ov; ovaries. Scale bars are of 100 µm.

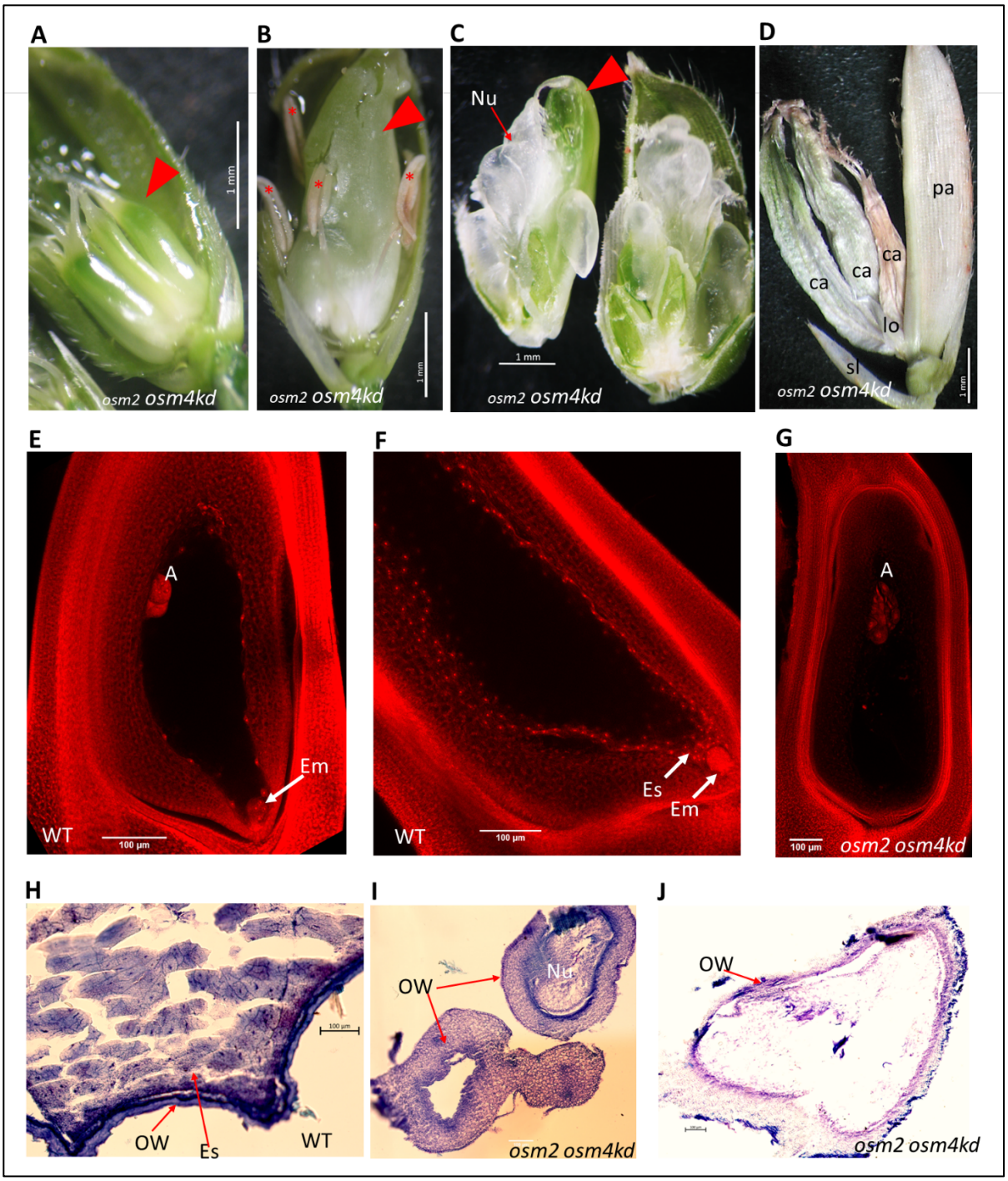

Figure 4. Parthenocarpy-like phenotypes in *osmads2*$^{d8/d8}$ *osmads4kd* double mutant. A and B, Pericarpic growth in double mutant florets of type I and type II phenotypes, respectively. The red arrowhead points at the expanded pericarp. In B, asterisks mark the indehiscent empty sterile anthers. The filaments of these sterile anthers failed to extend within the unopened florets. C, Floret of *osmads2*$^{d8/d8}$ *osmads4kd* double mutant with pericarpic growth. The growing ovary (red arrowhead) was manually dissected to show the over-proliferated nucellar mass inside (red arrow). D, Dry spikelet from *osmads2*$^{d8/d8}$ *osmads4kd* double mutant where lemma is removed to show the expanded pericarps that are shrunken and dry. E-G, Confocal microscopy Z-stacked images of ovaries from WT (E and F) and *osmads2*$^{d8/d8}$ *osmads4kd* double mutant (G). The double mutant ovary lacks embryo (Em) and endosperm (Es). H and I, Transverse section of WT and double mutant pericarps, respectively. J, Longitudinal section

of double mutant expanded pericarp. Unlike WT, the double mutant pericarp lacks granular endosperm. Abbreviation: Carpel (ca), lodicule (lo), palea (pl), sterile lemma (sl), ovary wall (OW). Scale bars: 1 mm in A-D, 100 µm in E-J.

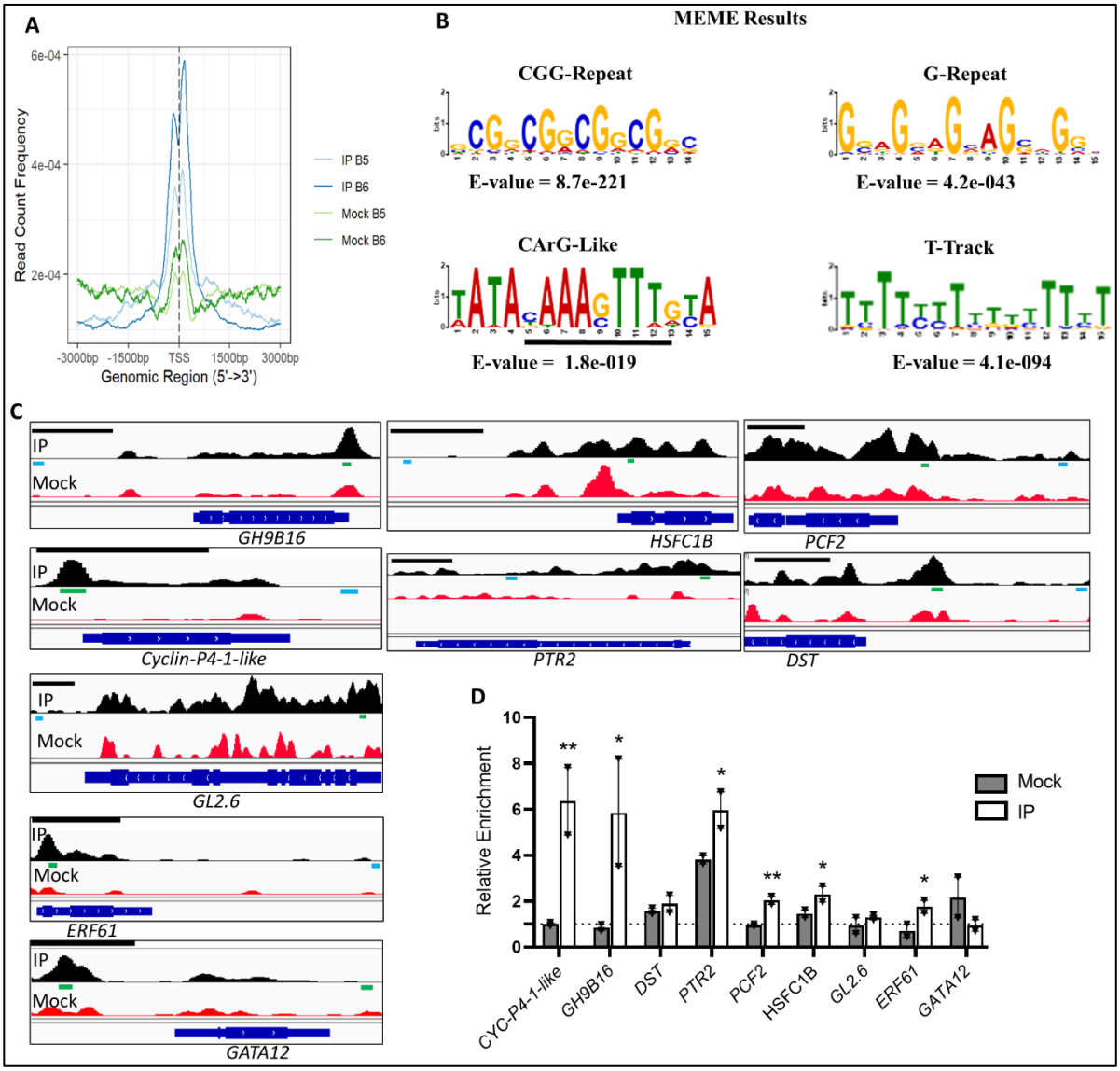

Figure 5: Analysis of genome-wide binding sites of OsMADS2 in WT panicles with developing florets. A, The plot shows relative distribution of OsMADS2 binding sites (ChIP-Seq peaks) mapped relative to TSS (from 3,000 bp upstream to 3,000 bp downstream). The blue lines represent peaks called by MACS2 algorithm using IP data over mock data. The green lines represent peaks called by MACS2 algorithm using Mock data over IP data. The Peaks of the IP over Mock show enrichment around the TSS. B, Significantly enriched motifs in the peak regions of the global data (MEME analysis). C and D, ChIP-qPCR based validation of some genomic loci bound by OsMADS2 in a pool of 0.5-1 cm inflorescences with developing florets. In C, a snapshot of IGV for each locus is shown where the ChIP-Seq peak regions and nonpeak regions (Control) are represented with green and cyan lines, respectively. The black line above each IGV tab is 1kb of the genome. In D, the bar plot represents the relative enrichment in IP and in mock. The relative enrichment (y-axis) is calculated by dividing the

%input of the peak region PCR to the %input of nonpeak control region PCR. The dotted line represents a threshold of 1 on the y-axis which corresponds to the %input values of the nonpeak control region PCR after being divided by themselves. The data are retrieved from two independent biological replicates, each includes 2 technical replicates. Values are means ± SEM. Significance of enrichment in IP over mock tested by multiple unpaired Student's *t* test. P <0.05 and P <0.001 are denoted as * and **, respectively.

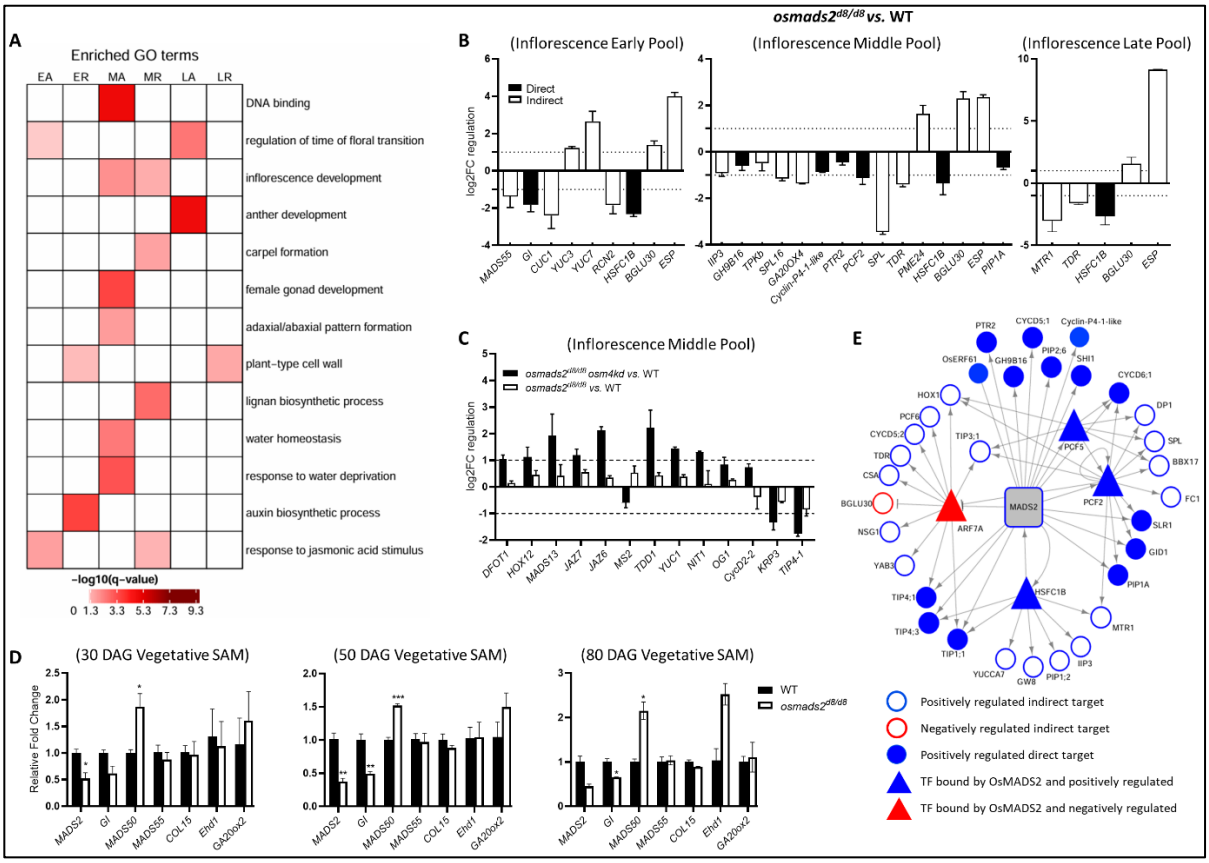

Figure 6. Gene ontology enrichment analysis and target genes regulated by OsMADS2. A, Heatmap representation of selected enriched GO terms in the differentially expressed gene sets. Oryzabase database (https://shigen.nig.ac.jp/rice/oryzabase/) GO annotation was used for this analysis and the significantly enriched GO terms were retrieved at qvalue ≤ 0.05. B and C, Plot representations of selected genes that are differentially expressed in panicles of early (0.2-0.5 cm), middle (0.5-1 cm) and late (1-2 cm) pools of *osmads2*$^{d8/d8}$, as per RT-qPCR based validation of the RNA-Seq data (B), and RT-qPCR analysis of candidate genes redundantly regulated by OsMADS2 and OsMADS4 in floral tissue pool constituting 0.5-1 cm inflorescences (C). Values are means ± SEM. The data are from two biological replicates of *osmads2* or two biological replicates of *osamds2*$^{d8/d8}$ *osmads4kd*, each includes 3 technical replicates. The average log2FC for three biological replicates of WT is equal to 0. The filled bars in panel B represent those genes that are deregulated as per RNA-seq and RT-qPCR data and bound by OsMADS2 as per ChIP-Seq analysis. D, graph plots displaying the relative expression of flowering time regulators interrogated by RT-qPCR in SAM (meristems and leaf primordia). Values are means ± SEM and derived from three biological replicates except for the plot of 80 DAG, the data are derived from two biological replicates. P <0.05, P <0.01d and

1373 P <0.001d denoted as *, ** and ***, respectively; Student's *t* test. E, A small Gene Regulatory
1374 Network (GRN) constructed based on ChIP-Seq data and transcriptome (RNA-Seq) data from
1375 panicles of 0.5-1 cm (termed here middle developmental pool). The small GRN displays subset
1376 of direct and indirect OsMADS2 target genes of annotated functions in osmotic regulation, cell
1377 cycle, cell wall modulation, auxin biosynthesis and other relevant to lodicule and stamen
1378 development. The full GRN is presented as Supplementary Fig. 14. The filled blue and red
1379 nodes represent positively- and negatively regulated direct downstream targets of OsMADS2,
1380 respectively. The unfilled circles in blue and red color boundaries represent genes positively
1381 and negatively regulated by OsMADS2, respectively. Triangle shape denotes nodal OsMADS2
1382 target genes coding for transcription factors (for e.g. PCF2 and PCF5) that were used to connect
1383 these direct target transcription factors to downstream DEGs that form the second layer in this
1384 GRN. The arrow shape and the T-shape indicate positive and negative regulation of each
1385 OsMADS2 gene target, respectively.

1386

1387

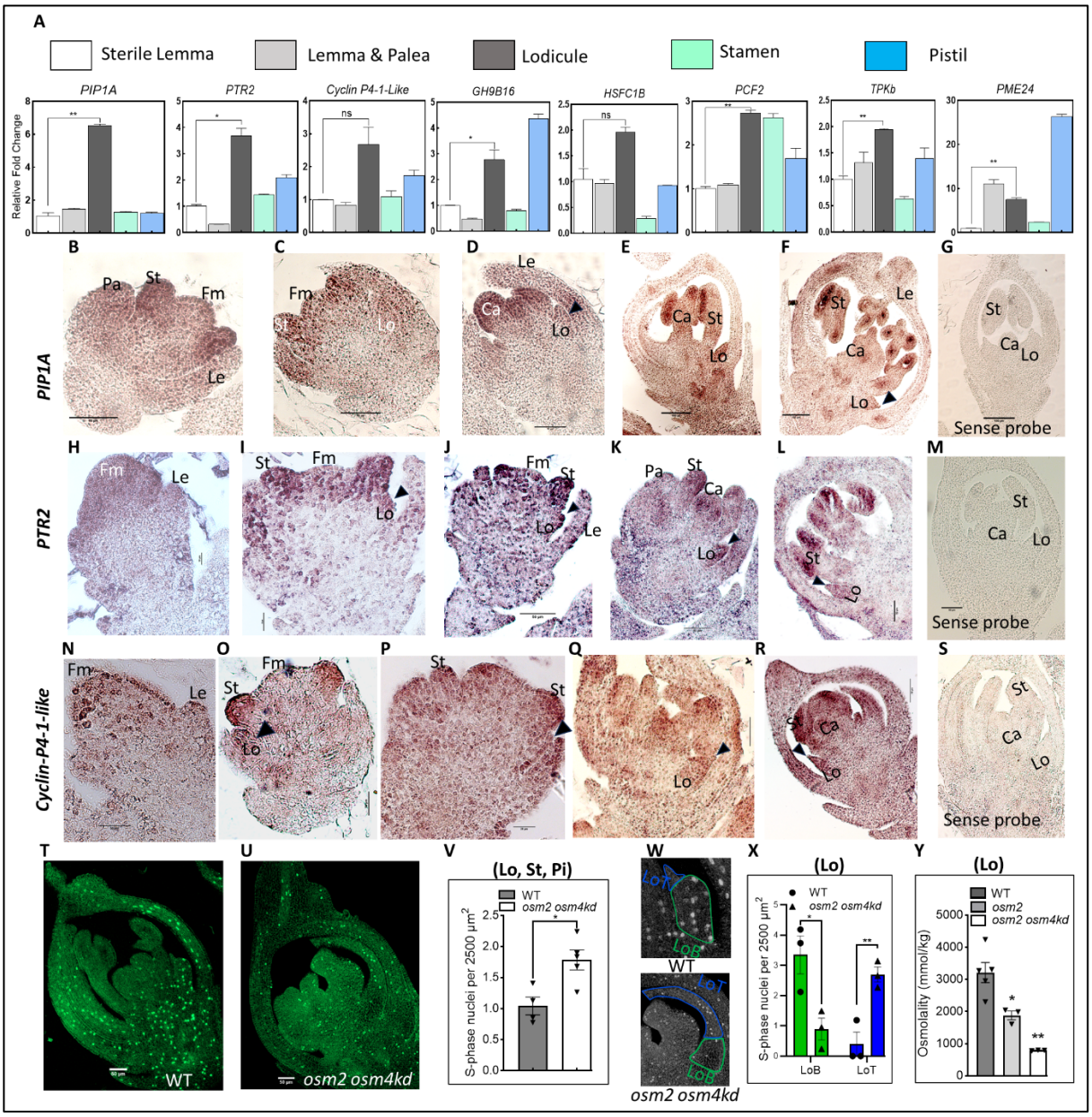

Figure 7. Spatiotemporal gene expression analysis of OsMADS2 targets and spatial distribution of S-phase cells in the developing floral organs. A, RT-qPCR analysis of lodicule developmentally relevant OsMADS2 gene targets examining their relative expression levels in the mature floral organs from pre-anthesis WT florets. The relative fold change is with respect to the expression in the sterile lemma. B-G, RNA *in situ* hybridization of *PIP1A* transcripts in developing WT florets. Sections in panels C-F and panel G are hybridized with antisense and sense probes, respectively. H-M, RNA *in situ* hybridization of *PTR2* transcripts in developing WT florets. Sections in panels H-L and panel M are hybridized with antisense and sense probes, respectively. N-S, RNA *in situ* hybridization of *Cyclin-P4-1-Like* transcripts in developing WT florets. Sections in panels N-R and panel S are hybridized with antisense and sense probes, respectively. The black arrowheads, in B-S, point at the lodicules. T and U, representative confocal micrographs of WT and *osmads2*$^{d8/d8}$ *osmads4kd* florets, respectively. The florets are of equivalent stages as inferred from their roughly equal dimensions. The S-phase nuclei (bright green signals) are labelled with 5-ethynyl-20 -deoxyuridine (EdU). V, Bar

graph plotting the number of S-phase cells per unit area, in the inner floral organs. W, confocal micrographs of WT and *osmads2*$^{d8/d8}$ *osmads4kd* lodicules demonstrating the distribution of S-phase cells in the lodicule body (LoB, green outlines) and lodicule tip (LoT, blue outlines). The whole florets are shown in panel T and U. X, Bar graph plotting the number of S-phase cells per unit area, in the lodicule body and the lodicule tip. Y, Comparison of osmolality levels in the cell sap from WT, *osmads2*$^{d8/d8}$ and *osmads2*$^{d8/d8}$ *osmads4kd* lodicules. Abbreviations: Fm, floral meristem, Le; lemma, Pa; palea, Lo; lodicule, St; stamen, Ca; carpel, Pi, pistil. Values are means ± SEM. P <0.05 and P <0.01d denoted as * and **, respectively; Student's *t* test. Scale bars: 20 in I, P; 50 µm in A-D, H, J-O, Q-U; 100 µm in E-G.

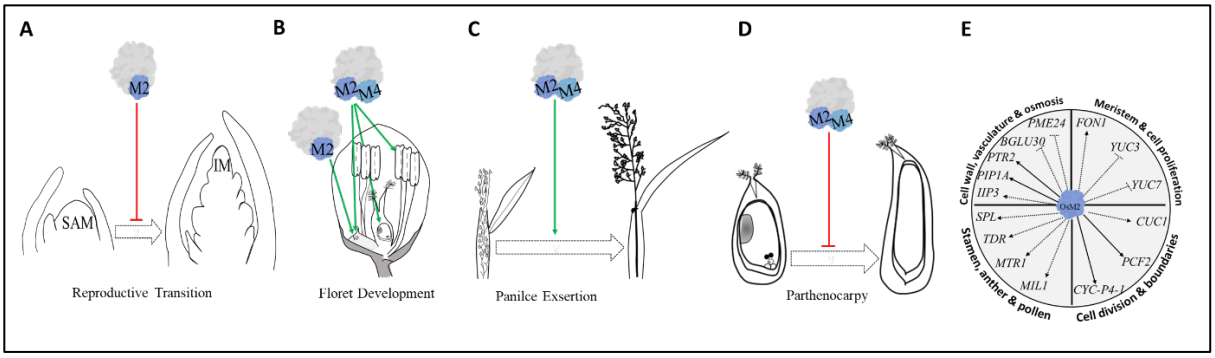

Figure 8. Graphical summary. A, OsMADS2 (M2) as part of a complex negatively regulates floral transition. B, OsMADS2 non-redudant role to promote normal lodicule development. Along with OsMADS4(M4) synergistically promotes normal lodicule, stamen and ovule development. C, OsMADS2 and OsMADS4 redundantly promotes inflorescence exsertion. D, OsMADS2 and OsMADS4 redundantly suppresses parthenocarpy. E, OsMADS2 regulates several downstream target genes that are annotated with functions in cell division, meristem size, meristem proliferation, cell wall modulation, vascular development, osmotic regulation, and stamen development. The solid lines and the dotted lines indicate direct and indirect regulation, respectively. The arrow shape and the T-shape indicate positive and negative regulation of each OsMADS2 gene target, respectively.